JOURNAL OF COLLOID AND INTERFACE SCIENCE **198,** 53–77 (1998)
ARTICLE NO. CS975266

The Effect of Ionic Strength on the Adsorption of H^+, Cd^{2+}, Pb^{2+}, and Cu^{2+} by *Bacillus subtilis* and *Bacillus licheniformis:* A Surface Complexation Model

Christopher J. Daughney,*[,1] and Jeremy B. Fein†

**Earth and Planetary Sciences, McGill University, 3450 University Street, Montréal, QC, H3A 2A7 Canada; and †Civil Engineering and Geological Sciences, University of Notre Dame, Notre Dame, Indiana, 46556-0767*

Received June 23, 1997; accepted October 24, 1997

To quantify metal adsorption onto bacterial surfaces, recent studies have applied surface complexation theory to model the specific chemical and electrostatic interactions occurring at the solution-cell wall interface. However, to date, the effect of ionic strength on these interactions has not been investigated. In this study, we perform acid–base titrations of suspensions containing *Bacillus subtilis* **or** *Bacillus licheniformis* **in 0.01 or 0.1 M $NaNO_3$, and we evaluate the constant capacitance and basic Stern double-layer models for their ability to describe ionic-strength-dependent behavior. The constant capacitance model provides the best description of the experimental data. The constant capacitance model parameters vary between independently grown bacterial cultures, possibly due to cell wall variation arising from genetic exchange during reproduction. We perform metal–** *B. subtilis* **and metal–** *B. licheniformis* **adsorption experiments using Cd, Pb, and Cu, and we solve for stability constants describing metal adsorption onto distinct functional groups on the bacterial cell walls. We find that these stability constants vary substantially but systematically between the two bacterial species at the two different ionic strengths.**

Key Words: **bacteria; metal; adsorption; ionic strength.**

INTRODUCTION

Bacteria and their cell wall fragments are ubiquitous in natural fluid-rock systems (1–9). Organic material often coats the mineral solids in such systems (10, 11), and so bacterial cell walls may represent a significant portion of the surface area exposed to both surface waters and soil fluids. Bacterial cell walls are known to exhibit a strong affinity for metal cations (12–18). The ubiquity of bacterial cells in near-surface fluid-rock systems and their ability to bind metals may play an important role in the subsurface transport of metals occurring as groundwater contaminants (19), the fossilization of microorganisms (20), and the accumulation of metal deposits (21). If such geochemical processes are to be quantified, a suitable model describing metal-bacteria interactions in natural environments must be developed.

Recent research indicates that the binding of protons and metal ions onto bacterial surfaces can be effectively described in terms of surface complexation, within the framework of equilibrium thermodynamics (15, 17, 18, 22). Acid–base titrations of bacterial suspensions permit the determination of the absolute concentrations and deprotonation constants of specific proton-active surface sites on the cell walls. Experimental studies of isolated systems containing a single metal and a single species of bacteria permit the determination of site-specific thermodynamic stability constants describing the formation of metal-bacteria surface complexes. For example, Fein *et al.* (17) suggest that the cell walls of *Bacillus subtilis* display carboxyl, phosphate, and hydroxyl functional groups, each in a different absolute concentration and each with a distinct deprotonation constant (Table 1). Fein *et al.* (17) also report stability constants describing the binding of various metals onto specific functional groups on the *B. subtilis* surface (Table 1). Daughney *et al.* (18) have performed a similar study using *Bacillus licheniformis* and noted that the concentrations of the functional groups, their deprotonation constants, and their metal-binding constants are slightly, but systematically, different from those of *B. subtilis* (Table 1). However, Fein *et al.* (17) and Daughney *et al.* (18) performed all of their experiments at a single, fixed ionic strength of 0.1 M, and so the effect of ionic strength on proton and metal adsorption by bacterial surfaces is unknown.

The adsorption of ions by bacterial surfaces is likely a function of ionic strength. Bacterial surfaces are often negatively charged in natural environments (23), and it is well established that ionic-strength-dependent electrostatic inter-

[1] To whom correspondence should be addressed. Fax: 514-398-4680. E-mail: chrisd@geosci.lan.mcgill.ca. Current address: Earth and Ocean Sciences, University of British Columbia, 6339 Stores Road, Vancouver, BC, V6T 1Z4 Canada.

0021-9797/98 $25.00

actions influence the adsorption of ions onto electrically charged surfaces (24, 25). The ionic strength dependence of ion adsorption onto mineral surfaces can be quantified by several different electrostatic models, each describing the distribution of electric potential at the mineral–water interface (26, 27). It is not clear, *a priori*, that these electrostatic models can be effectively applied to predict the extent of proton and metal adsorption by bacterial surfaces in electrolytes of differing ionic strengths.

The objective of this study, then, is to examine the effect of ionic strength on the acid–base properties (i.e., proton adsorption) and metal-binding capacities of two species of gram-positive bacteria, *B. subtilis* and *B. licheniformis*, both of which are common in natural environments (28). Using *B. subtilis* and *B. licheniformis* we perform acid–base titrations and batch metal adsorption experiments (with Cd, Pb, and Cu) in 0.01 M $NaNO_3$ electrolyte solutions. In conjunction with data from Fein *et al.* (17) and Daughney *et al.* (18), we compare the constant capacitance and basic Stern double-layer models in their ability to quantify ionic-strength-dependent adsorption behavior.

BACKGROUND AND THEORY

The cell walls of both *B. subtilis* and *B. licheniformis* are known to display active carboxyl, phosphate, and hydroxyl functional groups (16). The acid–base behavior displayed by these bacteria results from the sequential deprotonation of the cell wall functional groups with increasing pH (15, 17, 18, 22). The deprotonation of the carboxyl, phosphate, and hydroxyl surface functional groups may be represented by the equilibria

$$R - COOH^0 \Leftrightarrow R - COO^- + H^+ \quad [1]$$

$$R - PO_4H^0 \Leftrightarrow R - PO_4^- + H^+ \quad [2]$$

$$R - OH^0 \Leftrightarrow R - O^- + H^+, \quad [3]$$

where R represents the bacterial cell wall to which the functional group is attached. The mass action equations corresponding to the above equilibria are

$$K_{carb} = \frac{[R - COO^-]a_{H^+}}{[R - COOH^0]} \quad [4]$$

$$K_{phos} = \frac{[R - PO_4^-]a_{H^+}}{[R - PO_4H^0]} \quad [5]$$

$$K_{hydr} = \frac{[R - O^-]a_{H^+}}{[R - OH^0]}. \quad [6]$$

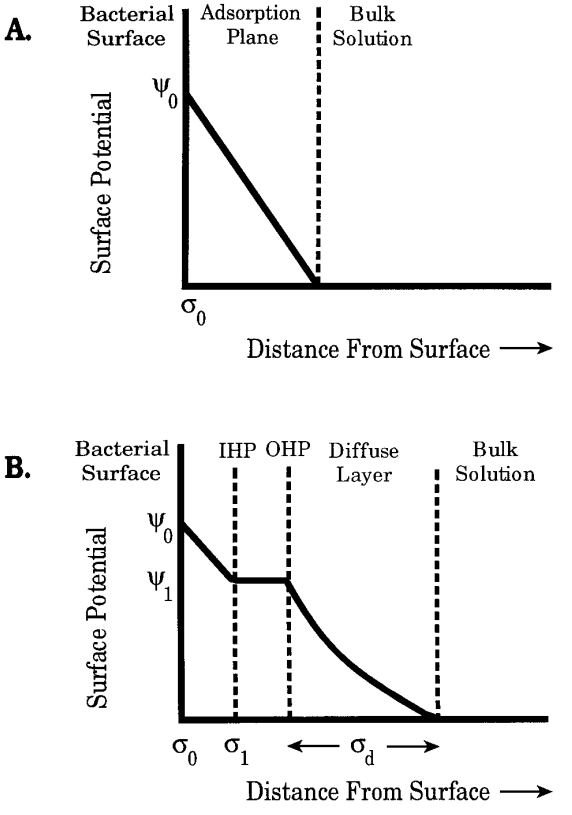

FIG. 1. Schematic representations of the distribution of electric potential (ψ) and electric charge (σ) at the bacterial surface–solution interface, for (A) the constant capacitance model and (B) the basic Stern model.

TABLE 1

Average Surface Characteristics and Metal-Binding Constants of *B. subtilis* and *B. licheniformis* as Determined by Fein *et al.* (17) and Daughney *et al.* (18)

Species	*B. subtilis*	*B. licheniformis*
Source	Fein *et al.* (17)	Daughney *et al.* (18)
Electrolyte	0.1 M $NaNO_3$	0.1 M $NaNO_3$
C_1[a]	8.0	3.0
pK_1[b]	4.8 ± 0.1	5.15 ± 0.3
Conc$_1$[c]	12.0 ± 1.0	8.88 ± 3.8
pK_2	6.9 ± 0.3	7.47 ± 0.4
Conc$_2$	4.4 ± 0.2	8.34 ± 4.6
pK_3	9.4 ± 0.3	10.17 ± 0.5
Conc$_3$	6.2 ± 0.2	12.7 ± 6.8
Log *K* Cd-carboxyl[d]	3.4 ± 0.1	3.85 ± 0.5
Log *K* Cd-phosphate	5.4 ± 0.2	4.35 ± 0.7
Log *K* Pb-carboxyl	4.2 ± 0.1	4.64 ± 0.3
Log *K* Pb-phosphate	5.6 ± 0.1	5.71 ± 0.7
Log *K* Cu-carboxyl	4.4 ± 0.1	4.88 ± 0.4
Log *K* Cu-phosphate	6.0 ± 0.2	—

[a] Capacitance of the bacterial surface (F/m^2).

[b] Negative logarithm and 1*s* error of the subscripted surface site, referenced to the condition of zero surface charge, zero surface coverage, and zero ionic strength. Subscripts 1, 2, and 3 correspond to carboxyl, phosphate, and hydroxyl functional groups, respectively.

[c] Concentration and 1*s* error of the subscripted surface functional group, expressed in $x10^{-5}$ mol per gram of bacteria.

[d] Logarithm and 1*s* error of stability constant describing adsorption of metal onto a particular surface functional group.

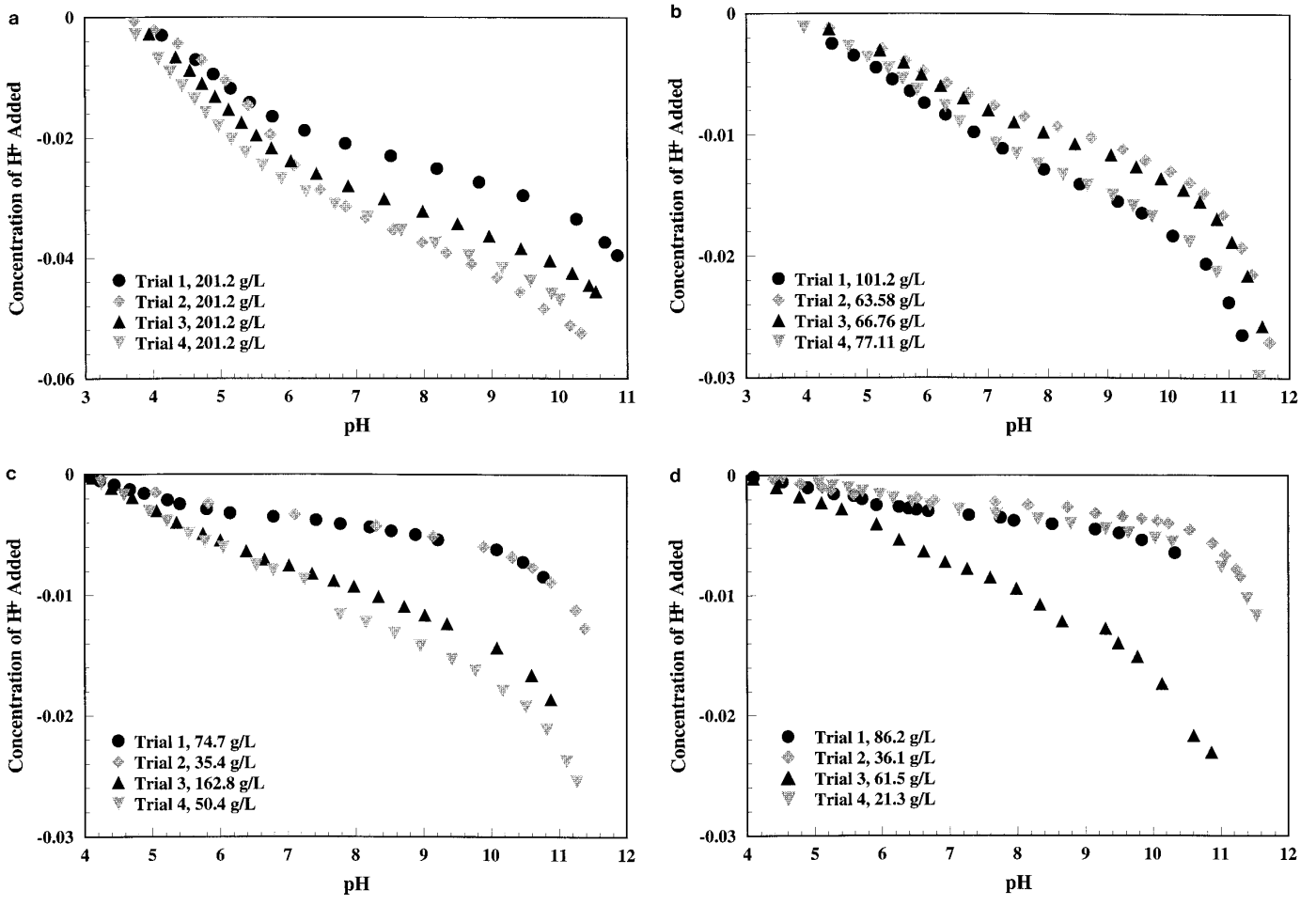

FIG. 2. Experimental data gathered during acid–base titration of (a) *B. subtilis* in 0.1 M $NaNO_3$ from Fein *et al.* (17), (b) *B. subtilis* in 0.01 M $NaNO_3$, (c) *B. licheniformis* in 0.1 M $NaNO_3$ from Daughney *et al.* (18), and (d) *B. licheniformis* in 0.01 M $NaNO_3$.

Here K and a represent the stability constant and the activity, respectively, and the square brackets represent the concentration of the surface species in moles per kilogram of solution. Stability constants for Eqs. [4]–[6] and total surface-site concentrations for each type of cell wall functional group for *B. subtilis* (17) and *B. licheniformis* (18) are presented in Table 1.

The adsorption of metal cations can be described by equilibria relating to the specific surface functional groups displayed on the cell wall:

$$M^m + R - COO^- \Leftrightarrow R - COOM^{(m-1)} \quad [7]$$

$$M^m + R - PO_4^- \Leftrightarrow R - PO_4M^{(m-1)} \quad [8]$$

$$M^m + R - O^- \Leftrightarrow R - OM^{(m-1)}. \quad [9]$$

The mass action equations corresponding to the above equilibria are

$$K_{M-\text{carb}} = \frac{[R - COOM^{(m-1)}]}{[R - COO^-]a_{M^m}} \quad [10]$$

$$K_{M-\text{phos}} = \frac{[R - PO_4M^{(m-1)}]}{[R - PO_4^-]a_{M^m}} \quad [11]$$

$$K_{M-\text{hydr}} = \frac{[R - OM^{(m-1)}]}{[R - O^-]a_{M^m}}. \quad [12]$$

The metal-binding stability constants for Eqs. [10]–[12], applicable to *B. subtilis* (17) and *B. licheniformis* (18), are also presented in Table 1. Fein *et al.* (17) and Daughney *et al.* (18) conclude that all surface complexes have a 1:1 stoichiometry, based on agreement between stability constant values determined in systems of differing bacteria to metal ratios. Further evidence in support of the 1:1 stoichiometry for the metal–bacteria surface complexes is provided by the electrophoretic mobility experiments of Collins and Stotzky (29), who report that bacterial cells, which are nega-

TABLE 2
Acid–Base Titration Data as Described by Individual Constant Capacitance Models

Trial[a]	g/L[b]	C_1[c]	pK_1[d]	Conc$_1$[e]	pK_2	Conc$_2$	pK_3	Conc$_3$	$V(Y)$[f]
				B. subtilis, 0.1 M $NaNO_3$					
1	201.2	3.3	4.80	1.01	7.38	3.67	9.82	7.38	1.4
2	201.2	4.4	4.98	9.45	5.88	8.60	8.60	8.03	9.3
3	201.2	4.1	4.73	12.8	6.88	40.8	9.14	5.90	1.4
4	201.2	8.0	4.51	13.2	6.44	4.68	8.75	5.48	1.6
Avr[g]		5.0	4.76	9.12	6.65	14.4	9.08	6.70	
1s[h]		2.1	0.2	5.7	0.6	18	0.5	1.2	
				B. subtilis, 0.01 M $NaNO_3$					
1	101.2	1.6	4.56	7.05	6.36	7.64	10.32	84.2	9.8
2	63.6	1.8	4.83	7.81	6.34	8.46	9.79	39.2	11.2
3	66.8	1.5	4.65	5.87	5.88	10.6	9.54	48.5	8.9
4	77.1	1.6	4.40	6.15	5.84	12.0	9.33	42.5	7.1
Avr		1.6	4.61	6.72	6.11	9.68	9.75	53.6	
1*s*		0.1	0.2	0.9	0.3	2.0	0.4	21	
				B. licheniformis, 0.1 M $NaNO_3$					
1	74.7	4.0	4.89	4.52	7.83	2.28	10.45	6.34	5.3
2	35.4	2.2	4.82	8.33	7.38	5.59	9.67	14.2	2.2
3	162.8	3.5	5.08	3.86	7.22	2.45	9.50	4.17	6.9
4	50.4	6.8	5.01	14.0	7.38	14.6	9.88	18.5	7.7
Avr[g]		4.1	4.95	7.68	7.45	6.23	9.85	10.8	
1s[h]		1.9	0.1	4.7	0.3	5.8	0.4	6.7	
				B. licheniformis, 0.01 M $NaNO_3$					
1	86.2	2.8	5.07	3.09	6.99	1.46	9.67	3.54	14.6
2	36.1	4.3	5.11	5.86	8.61	3.73	11.60	41.8	6.8
3	61.5	2.5	4.96	6.96	6.53	10.3	9.26	71.6	26.8
4	21.3	3.4	5.43	11.5	6.99	6.79	9.44	151	4.3
Avr		3.8	5.14	6.85	7.28	5.57	9.99	67.0	
1*s*		1.4	0.2	3.5	0.9	3.8	1.1	63	

[a] With the exception of the weight of bacteria per unit weight of electrolyte, the trials in each subset are identical replicates.
[b] Weight of bacteria per unit weight of electrolyte.
[c] Capacitance of the bacterial surface (F/m^2), treated as an optimizable parameter and adjusted to yield the lowest variance.
[d] Negative logarithm of the subscripted surface site, referenced to the ionic strength of the background electrolyte and zero surface charge.
[e] Concentration of the subscripted surface site, expressed in $x10^{-5}$ mol per gram of bacteria.
[f] Variance as calculated by FITEQL.
[g] Average values for all trials.
[h] 1*s* error corresponding to each average value.

tively charged in the absence of metals, become positively charged when divalent metals are present. The positive charge likely originates from a surface complex having one divalent metal ion coordinated to one surface functional group. Coordination of one metal ion to two surface functional groups, for example, would yield a surface complex with a neutral charge.

The bacterial surfaces, when deprotonated, carry a negative charge (23). The interaction between the metal cation and the electric charge surrounding the bacterial surface will affect all experimentally observed equilibrium constants ($K_{observed}$). We account for the electrostatic interactions with the relationship

$$K_{intrinsic} = K_{observed} \exp(zF\psi/RT). \quad [13]$$

Here, $K_{intrinsic}$ is the equilibrium constant referenced to the condition of zero surface charge, but to a distinct, finite ionic strength. The variables F, ψ, R, T, and z refer to Faraday's constant, the electric potential of the cell wall surface, the gas constant, the absolute temperature, and the charge of

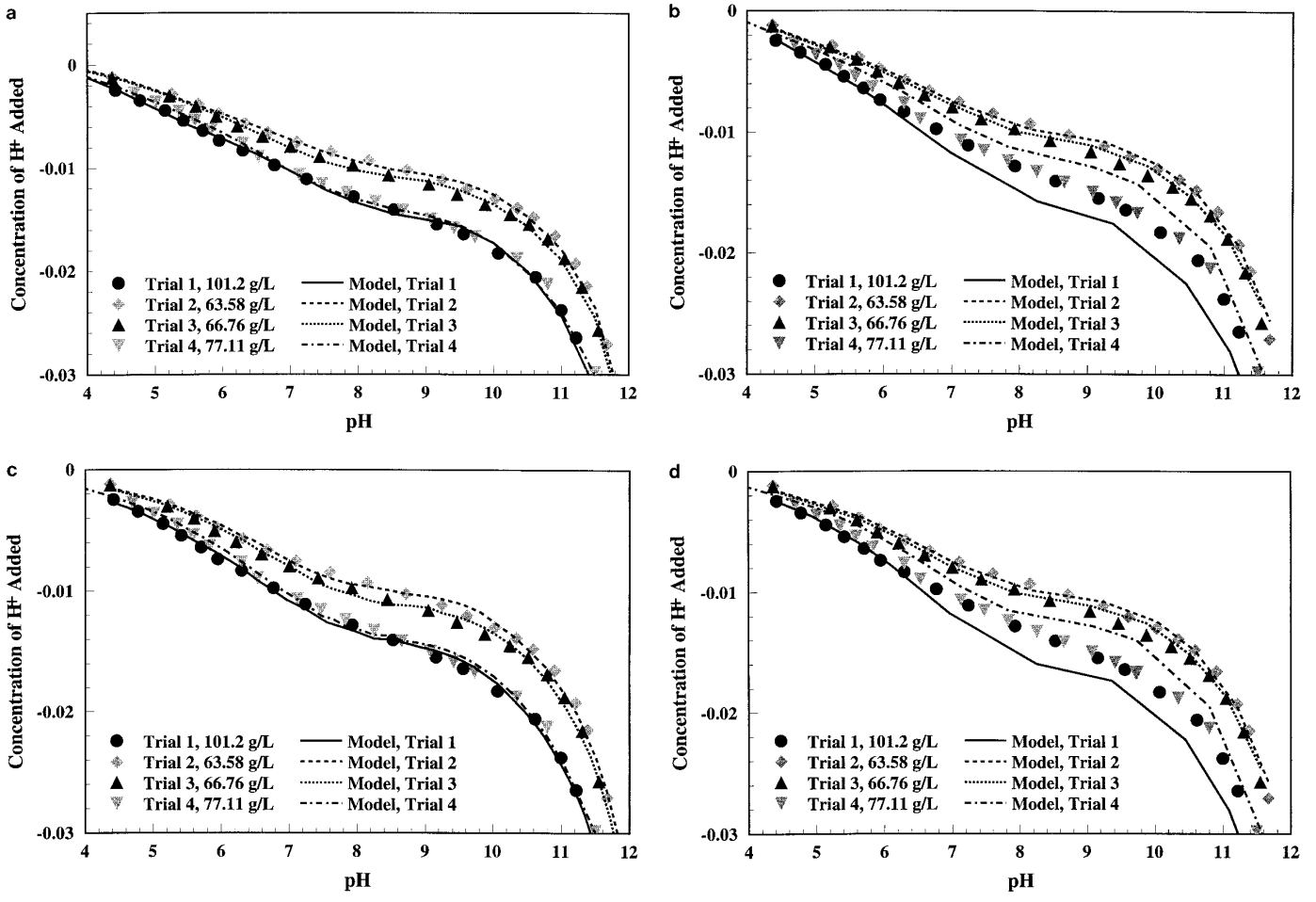

FIG. 3. FITEQL model curves describing acid–base behavior of B. subtilis in 0.01 M $NaNO_3$, for (a) individual constant capacitance models, (b) net constant capacitance models, (c) individual basic Stern models, and (d) net basic Stern models. The experimental data shown in all four graphs are identical to those of Fig. 2b.

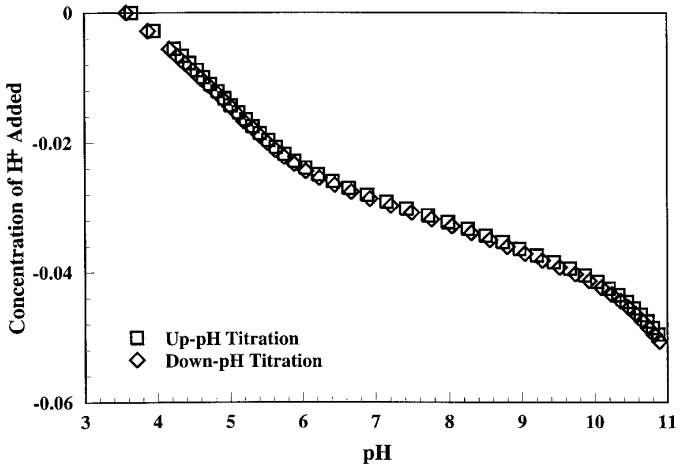

FIG. 4. Representative data gathered during an acid–base titration (of *B. subtilis* in 0.01 M $NaNO_3$) intended to test the reversibility of the proton adsorption–desorption reactions.

the adsorbing ion, respectively. The Boltzmann factor, $\exp(zF\psi/RT)$, quantifies the activity difference between an ion near the bacterial surface and the same ion in the bulk solution.

Several different electrostatic models have been developed to describe the configuration of the electric field surrounding charged surfaces in solution. In this study, we consider the constant capacitance model (30) and the basic Stern model (31). Schematic representations of the charge–potential relationships for these models are shown in Fig. 1. Both models have been used to describe metal and proton adsorption onto oxide mineral surfaces (26), and the constant capacitance model has been used to describe metal adsorption onto bacterial surfaces (17, 18). Both models are valid for the range of ionic strengths considered here, but they require optimization of a different number of parameters in order to describe experimental proton or metal adsorption data (32, 33). We do not consider the triple layer model (25), because it requires the optimization of parameters that

TABLE 3
Statistical Comparison of Individual Constant Capacitance Model Parameters

Parameter	Avr_1[a]	$1s_1$[b]	Avr_2	$1s_2$	f[c]	t[d]	CI[e]
Comparison of *B. subtilis* model parameters at 0.1[f] and 0.01[g] M							
C_1	5.0	2.1	1.6	0.1	6	1.617	<90%
pK_1	4.76	0.2	4.61	0.2	6	0.573	<60%
pK_2	6.65	0.6	6.11	0.3	6	0.773	<60%
pK_3	9.08	0.5	9.75	0.4	6	−0.971	<80%
$Conc_1$	9.12	5.7	6.72	0.9	6	0.419	<40%
$Conc_2$	14.4	18	9.68	2.0	6	0.265	<20%
$Conc_3$	6.70	1.2	53.6	21	6	−2.251	<95%
Comparison of *B. licheniformis* model parameters at 0.1[f] and 0.01[g] M							
C_1	4.1	1.9	3.8	1.4	6	0.127	<20%
pK_1	4.95	0.1	5.14	0.2	6	−0.815	<60%
pK_2	7.45	0.3	7.28	0.9	6	0.180	<20%
pK_3	9.85	0.4	9.99	1.1	6	−0.121	<20%
$Conc_1$	7.68	4.7	6.85	3.5	6	0.143	<20%
$Conc_2$	6.23	5.8	5.57	3.8	6	0.095	<20%
$Conc_3$	10.8	6.7	67.0	63	6	−0.893	<60%
Comparison of *B. subtilis*[f] and *B. licheniformis*[a] model parameters at 0.1 M							
C_1	5.0	2.1	4.1	1.9	6	0.318	<40%
pK_1	4.76	0.2	4.95	0.1	6	−0.845	<60%
pK_2	6.65	0.6	7.45	0.3	6	−1.158	<80%
pK_3	9.08	0.5	9.85	0.4	6	−1.136	<80%
$Conc_1$	9.12	5.7	7.68	4.7	6	0.197	<20%
$Conc_2$	14.4	18	6.23	5.8	6	0.439	<40%
$Conc_3$	6.70	1.2	10.8	6.7	6	−0.602	<60%
Comparison of *B. subtilis*[f] and *B. licheniformis*[g] model parameters at 0.01 M							
C_1	1.6	0.1	3.8	1.4	6	−1.567	<90%
pK_1	4.61	0.2	5.14	0.2	6	−1.970	<95%
pK_2	6.11	0.3	7.28	0.9	6	−1.229	<80%
pK_3	9.75	0.4	9.99	1.1	6	−0.206	<20%
$Conc_1$	6.72	0.9	6.85	3.5	6	−0.036	<20%
$Conc_2$	9.68	2.0	5.57	3.8	6	0.950	<80%
$Conc_3$	53.6	21	67.0	63	6	−0.203	<20%

[a] Average value and [b]1s error for each parameter in the subscripted variable set.
[c] Degrees of freedom.
[d] Value of the *t* distribution.
[e] Upper confidence level at which the average values can be considered statistically different.
[f] First and [g]second variable sets.

are not explicitly resolvable given the data collected in this study.

The constant capacitance model assumes that all adsorbed ions occupy an adsorption plane immediately adjacent to the solid surface (Fig. 1). The surface complexes formed are thus analogous to inner-sphere aqueous complexes. The electric potential in the zero plane (ψ_0) is related to the electric charge (σ_0) by the capacitance of the bacterial surface (C_1) (30):

$$C_1 = \frac{\sigma_0}{\psi_0}\,. \qquad [14]$$

Here, the surface potential is independent of ionic strength, and so the constant capacitance model cannot be used to predict changes in ion adsorption resulting from changes in ionic strength. Instead, the constant capacitance model requires a different set of surface deprotonation constants (Eqs. [4]–[6]) and metal-binding constants (Eqs. [10]–

TABLE 4
Summary of Net Constant Capacitance Model Parameters Computed from Simultaneous Modeling of All Titrations

Sp.[a]	I[b]	C_1[c]	pK_1[d]	Conc$_1$[e]	pK_2	Conc$_2$	pK_3	Conc$_3$	$V(Y)$[f]
B. sub.	0.1	8.0	4.76	11.0	6.65	5.35	9.08	4.22	334
	0.01	1.4	4.45	5.85	5.88	10.2	9.38	38.9	72.6
B. lich.	0.1	4.1	4.95	5.88	7.45	2.23	9.85	8.56	1540
	0.01	4.0	4.96	4.15	7.25	2.68	10.64	22.2	1798
Avr[g]		4.4	4.78	6.47	6.81	5.12	9.74	18.5	
1s[h]		2.7	0.2	3.1	0.8	3.7	16		

[a] Bacterial species.
[b] Ionic strength of $NaNO_3$ electrolyte.
[c] Capacitance of the bacterial surface (F/m^2), treated as an optimizable parameter.
[d] Negative logarithm of the subscripted surface site, referenced to the ionic strength of the background electrolyte and zero surface charge.
[e] Concentration of the subscripted surface site, expressed in $x10^{-5}$ mol per gram of bacteria.
[f] Variance as calculated at FITEQL.
[g] Average values for all models.
[h] 1*s* error corresponding to each average value.

[12]) for each ionic strength considered. In addition to the determination of pertinent stability constants, a description of metal–bacteria adsorption with the constant capacitance model requires determination of the total concentrations of the carboxyl, phosphate and hydroxyl functional groups. Finally, because the capacitance (C_1) cannot be measured directly, it must be considered a parameter for optimization.

The basic Stern model considers specifically adsorbed species to occupy either the inner Helmholtz plane (IHP), with capacitance C_1, or the outer Helmholtz plane (OHP), which is some distance away from the surface (the capacitance of OHP is omitted in the basic Stern model). Surface complexes in the IHP are again analogous to inner-sphere aqueous complexes, while surface complexes in the OHP are more similar to aqueous ion pairs, as the ions are only electrostatically bound to the surface. The OHP is the inner-

TABLE 5
Representative FITEQL Basic Stern Modeling for Two Individual *B. subtilis* Titrations

Model[a]	C_1[b]	pK_1[c]	Conc$_1$[d]	pK_2	Conc$_2$	pK_3	Conc$_3$	log K_{Na}	$V(Y)$[e]
				B. subtilis, 0.1 M $NaNO_3$, 201.2 g bacteria/L					
1p*K*	8.0	5.45	27.5	—	—	—	—	—	1614
1p*K* + Na	6.0	5.58	22.3	—	—	—	—	1.2	978
2p*K*	8.0	3.78	17.2	6.81	6.15	—	—	—	14.9
2p*K* + Na	5.9	4.31	15.2	6.77	7.15	—	—	0.4	3.6
3p*K*					No convergence[f]				
3p*K* + Na	3.9	5.05	14.4	6.20	4.80	8.16	7.82	1.55	0.1
				B. subtilis, 0.01 M $NaNO_3$, 63.6 g bacteria/L					
1p*K*	8.0	6.13	43.8	—	—	—	—	—	1183
1p*K* + Na	6.1	5.91	50.6	—	—	—	—	−2.7	1056
2p*K*	8.0	4.06	15.7	7.75	24.0	—	—	—	12.5
2p*K* + Na	4.0	3.98	15.9	7.65	33.6	—	—	−2.4	12.7
3p*K*					No convergence				
3p*K* + Na					No convergence				

[a] Models consider proton adsorption onto one, two, or three distinct types of surface functional groups, and are termed 1p*K*, 2p*K* and 3p*K*, respectively. Models considering Na^+ adsorption are indicated.
[b] Capacitance of the bacterial surface (F/m^2), treated as an optimizable parameter.
[c] Negative logarithm of the subscripted surface site, referenced to the ionic strength of the background electrolyte and zero surface charge.
[d] Concentration of the subscripted surface site, expressed in $x10^{-5}$ mol per gram of bacteria.
[e] Variance as calculated by FITEQL.
[f] Indicates severe misfit between the model and the experimental data.

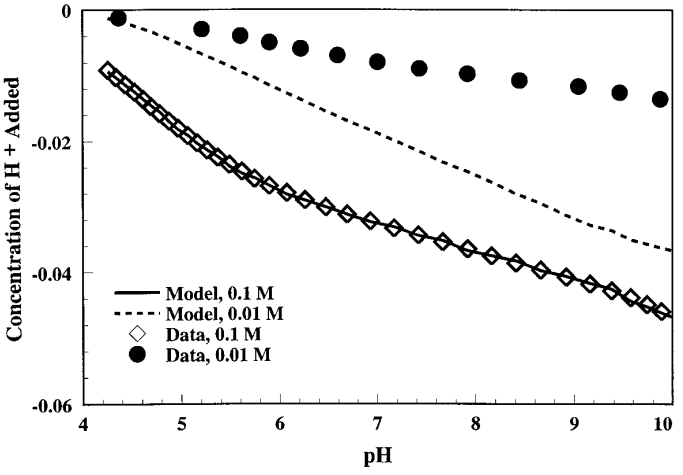

FIG. 5. Comparison of basic Stern model predictions and experimental data for two *B. subtilis* titrations. Model parameters were determined by fitting titration data for 0.1 M electrolyte; this model fails to match the 0.01 M titration data, when adjustments for ionic strength are made.

most plane of the diffuse layer. The relationships between charge (σ) and potential (ψ) in these planes are (31)

$$\sigma_0 = C_1(\psi_0 - \psi_1) \quad [15]$$

$$\sigma_1 = -\sigma_0 + \sigma_d = C_1(\psi_1 - \psi_0) + \sigma_d \quad [16]$$

$$\sigma_d = -0.1174\sqrt{I}\sinh(zF\psi_d/2RT). \quad [17]$$

Here, the subscripts 0, 1 and *d* denote the charge or potential at the surface, the IHP and the OHP, respectively, and I is the ionic strength of the solution. Unlike the constant capacitance model, the basic Stern model can predict adsorption over a wide range of ionic strengths with only one set of surface deprotonation constants. The Stern model accounts for changing ionic strength through Eq. [17] and by considering adsorption of electrolyte ions into the OHP. Because the bacterial surfaces are neutral or negatively charged, we consider adsorption of only the Na^+ electrolyte cations:

$$Na^+ + R - COO^- \Leftrightarrow R - COONa^0 \quad [18]$$

$$Na^+ + R - PO_4^- \Leftrightarrow R - PO_4Na^0 \quad [19]$$

$$Na^+ + R - O^- \Leftrightarrow R - ONa^0. \quad [20]$$

Corresponding stability constants for the above reactions are

$$K_{Na-carb} = \frac{[R - COONa^0]}{[R - COO^-]a_{Na^+}} \quad [21]$$

$$K_{Na-phos} = \frac{[R - PO_4Na^0]}{[R - PO_4^-]a_{Na^+}} \quad [22]$$

$$K_{Na-hydr} = \frac{[R - ONa^+]}{[R - O^-]a_{Na^+}}. \quad [23]$$

A full description of the adsorption of a single aqueous metal cation by the bacterial surface using the basic Stern model may require the determination of up to nine stability constants (Eqs. [4]–[6], [10]–[12], and [21]–[23]), one capacitance (C_1), and the total concentrations of the carboxyl, phosphate, and hydroxyl functional groups. All adsorbed ions may contribute to the potential of the surface, in turn controlling adsorption, and giving rise to a codependence between the stability constants describing the adsorption of metal ions and electrolyte ions. It is not possible to determine stability constants for Eqs. [4]–[6] and [21]–[23] simultaneously without measuring changes in the aqueous concetrations of both the metal ions and the electrolyte ions. Because the changes in the electrolyte concentration are very small, we measure only the changes in the metal concentration, and so several sets of stability constant values (Eqs. [4]–[6] and [21]–[23]) may fit the experimental data equally well (32).

In this study, we use the computer speciation program FITEQL 2.0 (34, 35) to calculate stability constants (Eqs. [4]–[6], [10]–[12], and [21]–[23]) and surface-site concentrations from experimental acid–base titration data. The FITEQL program used here has been modified by Johannes Lützenkirchen (Department of Inorganic Chemistry, Umea University, Sweden; personal communication) to accept a greater number of input data points and to consider input data for several different solid:solution ratios simultaneously. We attempt to describe the experimental data with several models involving different adsorption reactions, and FITEQL is used to compute a variance, $V(Y)$, which quantifies the fit of each model. The variance is normalized with respect to the number of experimental data points, the number of chemical components for which the total concentration is known, and the number of equilibrium constants to be determined, and so it provides a quantitative means of assessing the goodness of fit of the various models.

The thermodynamic standard states employed in this study for the solid phases and liquid water are taken to be the pure substance at 25°C and 1 atm. The standard state for aqueous species is a hypothetical one molal solution which exhibits the behavior of infinite dilution at the temperature and pressure of interest. Departures from this standard state are quantified by Davies equation activity coefficients. Neutral aqueous species are assigned activity coefficients of unity. The standard state for surface complexes is one of zero coverage and zero surface potential. Departures from this standard state are corrected with the Boltzmann equation, as outlined above. All equilibrium constants reported in this work are

TABLE 6
Acid–Base Titration Data as Described by Individual Basic Stern Models

Trial[a]	g/L[b]	C_1[c]	pK_1[3]	Conc$_1$[e]	pK_2	Conc$_2$	$V(Y)$[f]
			B. subtilis, 0.1 M $NaNO_3$				
1	201.2	8.0	4.42	12.1	7.97	7.18	43.9
2	201.2			No convergence[i]			
3	201.2	8.0	4.26	16.4	7.61	6.51	70.7
4	201.2	8.0	3.97	18.2	7.25	6.23	98.6
Avr[g]		8.0	4.22	15.6	7.61	6.64	
1s[h]		0.0	0.2	3.1	0.4	0.5	
			B. subtilis, 0.01 M $NaNO_3$				
1	101.2	2.7	3.85	14.1	7.91	57.9	11.3
2	63.6	8.0	4.11	15.9	7.81	25.3	19.8
3	66.8	8.0	4.12	16.7	7.83	25.2	20.0
4	77.1	8.0	3.95	18.1	7.55	24.1	20.2
Avr		6.7	4.01	16.2	7.73	33.1	
1s		2.7	0.1	1.7	0.3	17	
			B. licheniformis, 0.1 M $NaNO_3$				
1	74.7	8.0	4.76	5.19	8.19	4.17	35.3
2	35.4	4.5	4.61	10.8	7.95	13.7	17.3
3	162.8	5.5	5.08	5.04	8.02	4.90	33.8
4	50.4	8.0	4.66	24.5	7.29	19.8	86.3
Avr		6.5	4.78	11.4	7.86	10.6	
1s		1.8	0.2	9.2	0.4	7.5	
			B. licheniformis, 0.01 M $NaNO_3$				
1	86.2	8.0	4.76	4.38	8.18	4.33	78.4
2	36.1	8.0	4.30	6.79	7.96	9.26	89.8
3	61.5	12.0	4.57	19.4	7.84	8.99	135
4	21.3	8.0	4.38	19.6	7.36	17.9	112
Avr		9.0	4.50	12.5	7.84	10.1	
1s		2.0	0.2	8.1	0.4	5.7	

[a] With the exception of the weight of bacteria per unit weight of electrolyte, the trials in each subset are identical replicates.
[b] Weight of bacteria per unit weight of electrolyte.
[c] Capacitance of the bacterial surface (F/m^2).
[d] Negative logarithm of the subscripted surface site, referenced to the ionic strength of the background electrolyte and zero surface charge.
[e] Concentration of the subscripted surface site, in $x10^{-5}$ mol per gram of bacteria.
[f] Variance as calculated by FITEQL.
[g] Average values for all trials.
[h] 1s error corresponding to each average value.

referenced to 25°C, zero surface potential, and the ionic strength of the background electrolyte.

MATERIALS AND METHODS

Growth procedures. The bacteria were cultured as described by Fein *et al.* (17) and Daughney *et al.* (18). *B. licheniformis* and *B. subtilis* cells were obtained from T. J. Beveridge (University of Guelph, Ontario). The cells were cultured in 3-ml volumes of autoclaved (120°C for 20 min) trypticase soy broth (Becton Dickenson) containing 0.5 wt% yeast extract (Becton Dickenson). After growing for 24 h at 32°C, the cells were transferred to 1-L volumes of autoclaved broth and allowed to culture for an additional 24 h at 32°C. The cells were removed from the growth medium by centrifugation at 6000 rpm for 15 min. The pelleted cells were rinsed two times in distilled, deionized (DDI) water, soaked for 1 h in 0.1 M HNO_3, rinsed two times in DDI water, soaked overnight in 0.001 M EDTA, rinsed five times in DDI water, and finally rinsed two times in 0.01 M $NaNO_3$ (the electrolyte used in the experiments). Following each rinse, the cells were pelleted by centrifugation at 6000 rpm

TABLE 7
Statistical Comparison of Individual Basic Stern Model Parameters

Parameter	Avr_1[a]	$1s_1$[b]	Avr_2	$1s_2$	f[c]	t[d]	CI[e]
Comparison of *B. subtilis* model parameters at 0.1[f] and 0.01[g] M							
C_1	8.0	0.0	6.7	2.7	6	0.481	<40%
pK_1	4.22	0.2	4.01	0.1	6	0.939	<80%
pK_2	7.61	0.4	7.73	0.3	6	−0.254	<20%
$Conc_1$	15.6	3.1	16.2	1.7	6	0.419	<40%
$Conc_2$	6.64	0.5	33.1	17	6	0.265	<20%
Comparison of *B. licheniformis* model parameters at 0.1[f] and 0.01[g] M							
C_1	6.5	1.8	9.0	2.0	6	−0.929	<80%
pK_1	4.78	0.2	4.50	0.2	6	0.990	<80%
pK_2	7.86	0.4	7.84	0.4	6	0.035	<20%
$Conc_1$	11.4	9.2	12.5	8.1	6	−0.090	<20%
$Conc_2$	10.6	7.5	10.1	5.7	6	0.053	<20%
Comparison of *B. subtilis*[f] and *B. licheniformis*[g] model parameters at 0.1 M							
C_1	8.0	0.0	6.5	1.8	6	0.833	<60%
pK_1	4.22	0.2	4.78	0.2	6	−1.980	<95%
pK_2	7.61	0.4	7.86	0.4	6	−0.442	<40%
$Conc_1$	15.6	3.1	11.4	9.2	6	0.433	<40%
$Conc_2$	6.64	0.5	10.6	7.5	6	−0.527	<40%
Comparison of *B. subtilis*[f] and *B. licheniformis*[g] model parameters at 0.01 M							
C_1	6.7	2.7	9.0	2.0	6	−0.685	<60%
pK_1	4.01	0.1	4.50	0.2	6	−2.191	<95%
pK_2	7.73	0.3	7.84	0.4	6	−0.220	<20%
$Conc_1$	16.2	1.7	12.5	8.1	6	0.447	<40%
$Conc_2$	33.1	16.5	10.1	5.7	6	1.318	<80%

[a] Average value and [b]1*s* error for each parameter in the subscripted variable set.
[c] Degrees of freedom.
[d] Value of the *t* distribution.
[e] Upper confidence level at which the average values can be considered statistically different.
[f] First and [g]second variable sets.

for 15 min, and the supernatant was discarded. This procedure was followed in order to strip the cell walls of any metals present in the growth medium.

Acid–base titrations. Acid–base titrations were performed in order to determine the deprotonation constants and absolute concentrations of the specific functional groups present on the bacterial cell walls. The bacterial cells were suspended in 10.0 ml of 0.1 or 0.01 M $NaNO_3$, which had been bubbled with N_2 for 60 min in order purge it of dissolved CO_2. The titration vessel was sealed immediately, and a positive internal pressure of N_2 was maintained for the duration of the experiment. The titrations were conducted using a Radiometer-Copenhagen TTT85-autotitrator/ABU80-burette assembly. The pH of the bacterial suspension was recorded after each addition of titrant (1.00 or 0.50 M NaOH, standardized against reagent-grade K–H–phthalate) only when a stability of 0.1 mV/s had been attained. Following the titration, the bacteria present in the titration vessel were pelleted by centrifugation at 6000 rpm for 60 min, and the weight of the dry pellet was recorded. High-performance liquid chromatography (HPLC) was used to analyze the supernatants for dissolved organic exudates. Four titrations were performed for each bacterial species at each ionic strength.

Adsorption experiments. Batch experiments were conducted as a function of pH in order to determine site-specific stability constants for Cd, Pb, and Cu adsorption onto the bacterial surfaces. The washed bacteria were pelleted by centrifugation at 6000 rpm for 60 min. The bacterial pellet was weighed and then resuspended in a known weight of 0.1 or 0.01 M $NaNO_3$ electrolyte to yield a parent suspension. Homogeneous 5.00-g aliquots of this parent suspension together with a known volume of 1000 ppm aqueous metal standard (Cd, Pb, or Cu) were added to several identical

TABLE 8
Summary of Net Basic Stern Model Parameters Computed from Simultaneous Modeling of All Titrations

Sp.[a]	I[b]	C_1[c]	pK_1[d]	Conc$_1$[e]	pK_2	Conc$_2$	$V(Y)$[f]
B. sub.	0.1	8.0	4.22	14.5	7.61	7.37	563
	0.01	8.0	4.10	16.4	7.78	21.4	84.8
	All			No convergence[g]			
B. lich.	0.1	8.0	4.87	6.06	9.07	17.2	1650
	0.01	8.0	4.50	5.72	9.30	5.28	1772
	All	8.0	4.84	5.61	9.75	5.60	1582
Avr[h]	All	8.0	4.51	9.66	8.70	11.4	
1s[i]			0.4	5.3	1.0	7.4	

[a] Bacterial species.
[b] Ionic strength of $NaNO_3$ electrolyte. ''All'' refers to FITEQL model which considers both ionic strengths and all solid:solution ratios.
[c] Negative logarithm of the subscripted surface site, referenced to the ionic strength of the background electrolyte and zero surface charge.
[d] Concentration of the subscripted surface site, expressed in $x10^{-5}$ mol per gram of bacteria.
[e] Capacitance for the bacterial surface (F/m^2).
[g] Indicates severe misfit between the model and the experimental data.
[h] Average values for all models.
[i] 1*s* error corresponding to each average value.

reaction vessels, and the pH of the suspension in each vessel was adjusted to a different value using 1.0 M HNO_3 or NaOH. The reaction vessels were shaken and allowed to equilibrate for 30 min. The 30-min reaction time was chosen based on the kinetic experiments reported by Fein *et al.* (17). The contents of each reaction vessel were then filtered through a 0.45-μm cellulose nitrate/acetate filter (Micron Separation Inc.). The filtrate from each reaction vessel was acidified and analyzed for the dissolved metal by flame atomic absorption spectrophotometry. Experiments for the Cd, Pb, and Cu systems were repeated in duplicate, with 1.5, 3.5, or 6.0 g of bacteria per liter of suspension, and total metal concentrations ranged from 10 to 35 ppm.

PROTON ADSORPTION RESULTS AND DISCUSSION

Experimental data collected during acid–base titrations of *B. subtilis* and *B. licheniformis* in 0.1 and 0.01 M $NaNO_3$ indicate that the bacteria impart significant buffering capacity to the suspensions between pH 3 and 12 (Fig. 2). In the following section, we compare the constant capacitance and basic Stern models in their ability to describe the experimental titration data and predict ionic-strength-dependent behavior. First, we model each of the 16 titrations individually, examining the extent to which the optimizable model parameters vary between the different trials. Next, we simultaneously model the 4 titrations of a given bacteria in a particular electrolyte, in order to derive a single set of optimizable model parameters applicable to all solid:solution ratios (but a single ionic strength). This set of parameters should, in theory, correspond closely to the average of the parameters determined by modeling the 4 titrations individually. Finally,

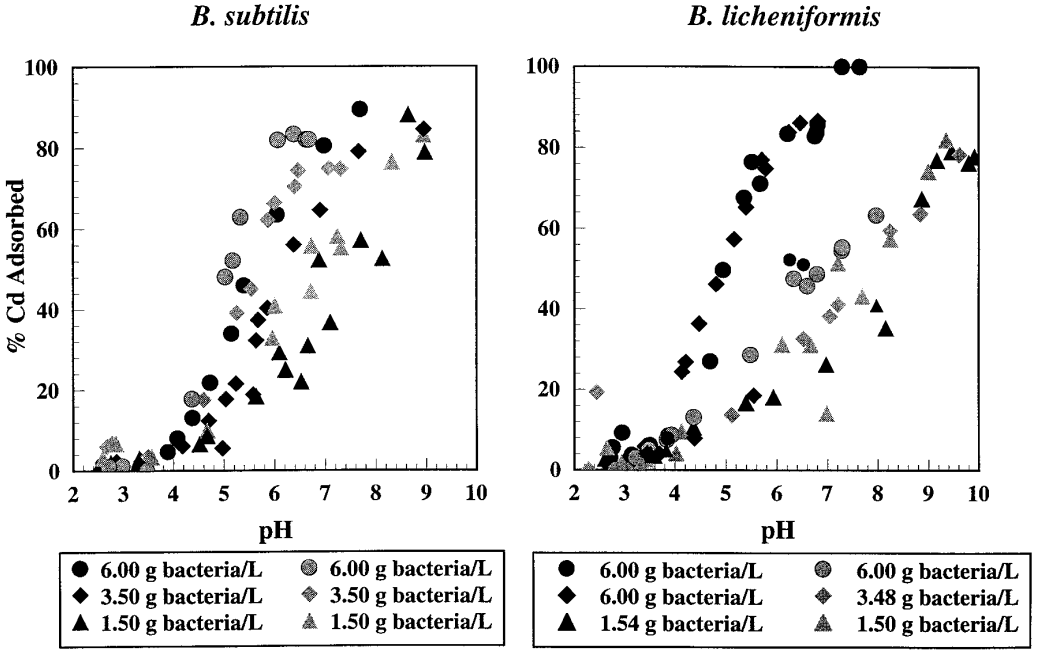

FIG. 6. Percentage adsorption of Cd^{2+} onto *B. subtilis* and *B. licheniformis* in 0.1 M $NaNO_3$ (black symbols) and 0.01 M $NaNO_3$ (gray symbols). Experiments are performed with two, independently grown bacterial cultures. Experimental solutions contain 10 ppm Cd.

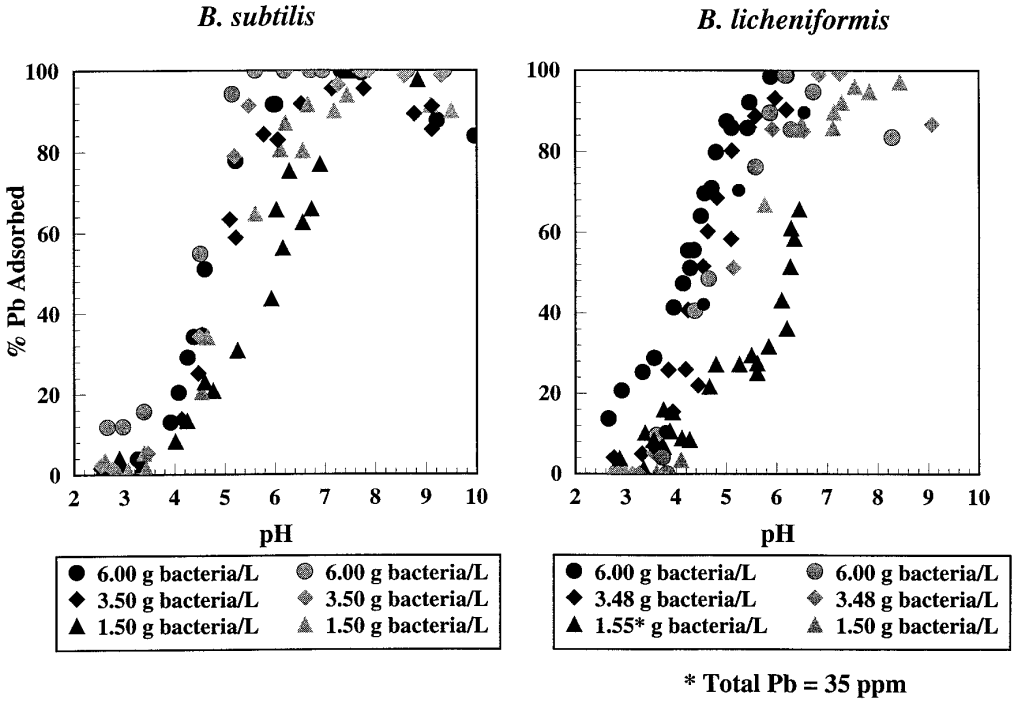

FIG. 7. Percentage adsorption of Pb^{2+} onto *B. subtilis* and *B. licheniformis* in 0.1 M $NaNO_3$ (black symbols) and 0.01 M $NaNO_3$ (gray symbols). Experiments are performed with two, independently grown bacterial cultures. Experimental solutions contain 10 ppm Pb unless otherwise noted.

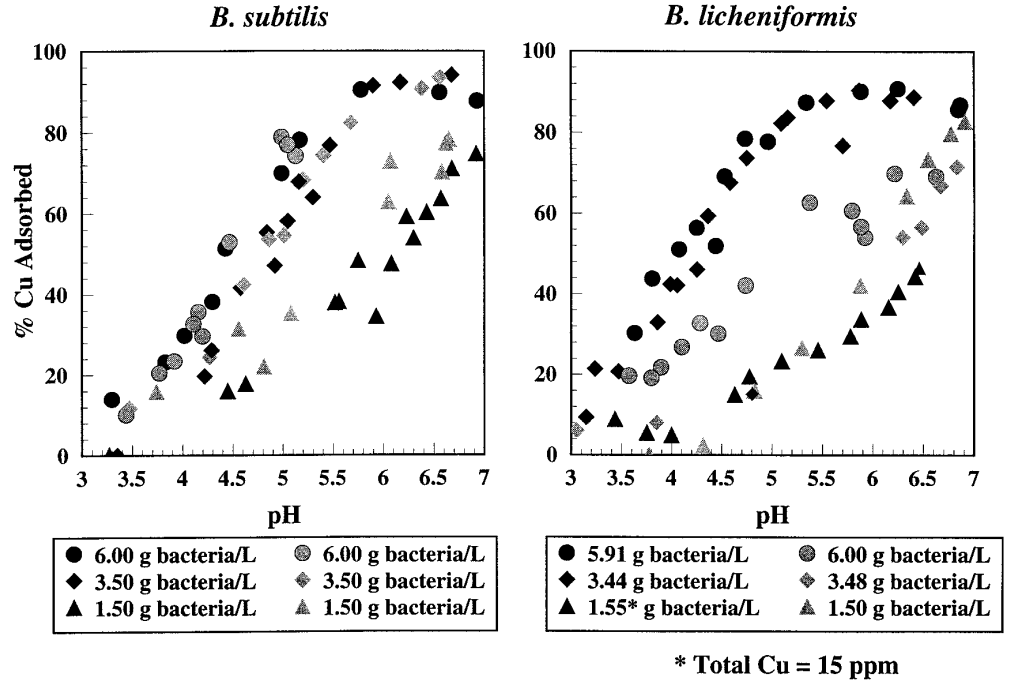

FIG. 8. Percentage adsorption of Cu^{2+} onto *B. subtilis* and *B. licheniformis* in 0.1 M $NaNO_3$ (black symbols) and 0.01 M $NaNO_3$ (gray symbols). Experiments are performed with two, independently grown bacterial cultures. Experimental solutions contain 10 ppm Cu unless otherwise noted.

TABLE 9a

Adsorption of Cd^{2+} by *B. subtilis* as Modeled by FITEQL, Treating Each Bacteria:Metal Ratio Independently

	6.0 g bacteria/L, 10 ppm Cd[b]			3.5 g bacteria/L, 10 ppm Cd			1.5 g bacteria/L, 10 ppm Cd		
Model[a]	Log K_1[c]	Log K_2[d]	$V(Y)$[e]	Log K_1	Log K_2	$V(Y)$	Log K_1	Log K_2	$V(Y)$
				Cd^{2+}–*B. subtilis* adsorption, 0.1 M $NaNO_3$					
C	3.05	—	26.6	3.08	—	39.7	3.54	—	76.9
P	4.67	—	9.5	4.39	—	12.0	4.43	—	27.7
H	7.21	—	11.9	6.89	—	20.9	6.66	—	23.2
C + P	2.78	4.09	0.6	2.69	4.02	1.5	2.34	4.36	29.7
C + H	2.84	6.38	2.23	2.81	6.21	4.0	3.07	5.85	14.6
P + H		No convergence[f]			No convergence			No convergence	
				Cd^{2+}–*B. subtilis* adsorption, 0.01 M $NaNO_3$					
C	2.97	—	4.1	2.95	—	39.7	3.18	—	18.1
P	3.42	—	10.7	3.11	—	12.0	2.90	—	17.8
H	6.56	—	14.2	6.17	—	20.9	5.29	—	76.2
C + P		No convergence			No convergence		2.91	2.28	14.6
C + H		No convergence			No convergence		3.06	3.50	7.9
P + H		No convergence			No convergence		2.84	3.27	15.6

[a] Models consider adsorption onto one or two distinct types of surface functional groups. C, carboxyl site; P, phosphate site; H, hydroxyl site.
[b] Composition of experimental solutions, indicating mass of bacteria per unit weight of electrolyte and total concentration of metal.
[c] Log K value for metal adsorption onto the first type of surface site included in the model column, referenced to the condition of zero surface charge and zero surface coverage and the ionic strength of the background electrolyte.
[d] Log K value for metal adsorption onto the second type of surface site considered in the model column.
[e] Variance as calculated by FITEQL.
[f] Indicates severe misfit between the model and the experimental data.

we simultaneously model all 8 titrations of each bacteria, in order to determine a parameter set which can be applied to all solid:solution ratios and both ionic strengths. Note that the basic Stern model can be applied in this last case, because the charge-potential relationship is ionic strength dependent, but the constant capacitance model cannot.

For each model proposed, we use FITEQL to solve up to 10 optimizable parameters: the capacitance of the bacterial surface, the deprotonation constants (Eqs. [4]–[6] for the constant capacitance model, Eqs. [4]–[6] and [21]–[23] for the basic Stern model), and absolute concentrations (mol/L) of each of the three types of surface functional groups. The concentrations of the functional groups can be normalized with respect to the weight of bacteria per unit weight of electrolyte to yield concentrations in moles per gram of bacteria. Equilibria describing the aqueous dissociation of water, the acid, the base, and the electrolyte are included in the model, with stability constants taken from Smith and Martell (36).

Constant capacitance models. We first model the acid–base behavior of the 16 titrations individually, using the constant capacitance model (FITEQL models are summarized in Table 2 and compared to the experimental data in Fig. 3). Fein *et al.* (17) and Daughney *et al.* (18) have used the constant capacitance model to describe the acid–base behavior of *B. subtilis* and *B. licheniformis* in 0.1 M $NaNO_3$, applying models which consider three distinct types of proton-active surface functional groups, as described above. Similarly, the experimental data presented here are better described by models involving three distinct proton-active sites than by models considering only one or two types of proton-active sites, and so parameters for the one-site and two-site models are not tabulated here.

The variances for these individual constant capacitance models are small, indicating an excellent correlation between the model and the experimental data. However, because each titration is modeled independently, the optimizable parameters can vary between trials. The average values and standard deviations (1s) displayed in Table 2 indicate that there is substantial variation in the relative and absolute concentrations of the cell wall functional groups of both *B. subtilis* and *B. licheniformis.* The cell wall structures of both species are known to change if the growth conditions are varied (37), but our experimental procedure ensures that growth conditions are controlled and reproducible. We have verified our method of titration by reproducing the stability constant and absolute concentration of functional groups in a sodium acetate system. An examination of the bacterial suspensions by HPLC and optical microscopy both before and after the titration gives no evidence of organic exudates or cell wall

TABLE 9b

Adsorption of Cd^{2+} by *B. licheniformis* as Modeled by FITEQL, Treating Each Bacteria:Metal Ratio Independently

	6.0 g bacteria/L, 10 ppm Cd[b]			3.5 g bacteria/L, 10 ppm Cd			1.5 g bacteria/L, 10 ppm Cd		
Model[a]	Log K_1[c]	Log K_2[d]	$V(Y)$[e]	Log K_1	Log K_2	$V(Y)$	Log K_1	Log K_2	$V(Y)$
				Cd^{2+}–*B. licheniformis* adsorption, 0.1 M $NaNO_3$					
C	4.00	—	26.6	3.98	—	6.4	4.25	—	131
P	6.39	—	11.7	6.59	—	8.7	5.92	—	155
H	8.07	—	13.0	8.31	—	14.9	5.37	—	51.7
C + P	3.62	5.79	10.7	3.86	5.48	1.2		No convergence[f]	
C + H	3.73	7.29	11.6	3.88	7.16	1.3	3.58	5.09	5.6
P + H		No convergence			No convergence		5.63	4.73	18.6
				Cd^{2+}–*B. licheniformis* adsorption, 0.01 M $NaNO_3$					
C	3.49	—	7.1	3.71	—	56.2	4.37	—	100
P	4.43	—	47.4	4.45	—	30.6	5.42	—	100
H	6.71	—	71.2	6.41	—	63.3	6.56	—	78.4
C + P	3.39	3.50	4.8	3.10	4.20	26.5		No convergence	
C + H	3.43	5.31	5.0	3.49	4.97	24.3	3.98	5.69	28.2
P + H		No convergence		4.37	4.24	28.3	5.04	5.39	43.0

[a] Models consider adsorption onto one or two distinct types of surface functional groups. C, carboxyl site; P, phosphate site; H, hydroxyl site.
[b] Composition of experimental solutions, indicating mass of bacteria per unit weight of electrolyte and total concentration of metal.
[c] Log K value for metal adsorption onto the first type of surface site included in the model column, referenced to the condition of zero surface charge and zero surface coverage and the ionic strength of the background electrolyte.
[d] Log K value for metal adsorption onto the second type of surface site considered in the model column.
[e] Variance as calculated by FITEQL.
[f] Indicates severe misfit between the model and the experimental data.

disruption. Further, the titrations are reversible (Fig. 4), suggesting that the extremes in pH do not cause changes in the cell wall structure through saponification of lipids or destruction of peptide bonds. Thus we conclude that the observed variation in surface-site concentrations is due to true variation in the cell wall structure. Both *B. subtilis* and *B. licheniformis* are capable of forming spores, and the composition of the spore wall is known to differ from that of the cell wall (38). The duration of the titrations may be sufficient to allow varying degrees of sporulation in response to changes in solution chemistry, giving rise to the observed variation in surface-site concentration. However, because the extent of variation is not systematic for a given type of site, a given ionic strength, or a given bacterial species, we suggest that the variations in surface-site concentrations are due to essentially random differences in cell wall structure arising from genetic mutation during reproduction.

The variations in the log stability constants are small relative to the variations in the surface-site concentrations. This limited variability suggests either that the deprotonation of a given functional group is not affected by changes in the surrounding cell wall structure, or that there are simply so many functional groups on the cell wall that an average value is appropriate. The variation in the deprotonation constants is smallest for the carboxyl sites and largest for the hydroxyl sites. This trend may reflect greater local cell wall variation around the hydroxyl sites. However, because the hydroxyl site concentrations do not vary significantly more than the concentrations of the other sites, this trend is more likely to be caused by experimental errors, which increase with pH due to a decrease in the buffering capacity of the bacterial suspensions.

The capacitance of the bacterial surface is also treated as an optimizable parameter. For each individual titration, we use FITEQL to determine the capacitance value which yields the lowest variance. The best-fitting capacitance varies between titrations, but this variation is of questionable significance, because the values of the capacitance and the total concentrations of surface sites are not independently resolvable. The concentrations of the functional groups can be inferred from the experimental data describing proton adsorption, and thus the bacterial surface charge can be calculated. However, it is the electric potential of the surface, rather than the charge, which directly affects the observed proton adsorption, through Eq. [13]. The surface electric potential cannot be determined directly, and so must be related to the surface charge through the surface capacitance, using Eq. [14]. Thus, a change in the total concentration of proton-active sites will cause a corresponding change in the value of the model capacitance. Therefore, we suggest that

TABLE 9c

Adsorption of Cd^{2+} by *B. subtilis* and *B. licheniformis* as Modeled by FITEQL, with All Bacteria:Metal Ratios Modeled Simultaneously

	0.1 M $NaNO_3$			0.01 M $NaNO_3$		
Model[a]	Log K_1[b]	Log K_2[c]	$V(Y)$[d]	Log K_1	Log K_2	$V(Y)$
			Cd^{2+}–*B. subtilis* adsorption			
C	3.19	—	68.7	3.02	—	12.1
P	4.48	—	18.2	3.44	—	25.4
H	6.95	—	23.6	6.16	—	65.6
C + P	2.67	4.19	11.1	2.93	2.39	9.9
C + H	2.86	6.16	7.0	2.98	3.54	7.3
P + H	4.44	4.45	16.3	3.43	2.65	26.1
			Cd^{2+}–*B. licheniformis* adsorption			
C	4.06	—	54.4	3.75	—	83.7
P	6.48	—	56.2	4.64	—	72.5
H	7.98	—	68.1	6.56	—	69.4
C + P	3.87	5.06	28.1	3.36	4.24	54.9
C + H	3.94	5.02	16.0	3.49	2.26	29.2
P + H	6.47	4.72	16.1	4.49	5.28	49.0

[a] Models consider adsorption onto one or two distinct types of surface functional groups. C, carboxyl site; P, phosphate site; H, hydroxyl site.

[b] Log K value for metal adsorption onto the first type of surface site included in the model column, referenced to the condition of zero surface charge and zero surface coverage and the ionic strength of the background electrolyte.

[c] Log K value for metal adsorption onto the second type of surface site considered in the model column.

[d] Variance as calculated by FITEQL.

the observed variation in the best-fit capacitance is due to true variation in the relative and absolute concentrations of the cell wall functional groups. The range of capacitance values used here ($1.5–8.0\ F/m^2$) alters the model determination of site concentrations and deprotonation constants by less than 5%.

We apply the Student t test (39) for averages to evaluate the significance of the parameter variation between individually modeled titrations,

$$t = \frac{X_1 - X_2}{\sqrt{s_1^2 + s_2^2}}, \qquad [24]$$

where X and s are the mean value and the standard deviation of the subscripted population, respectively. For a given degree of freedom (f, where $f = n_1 + n_2 - 2$, and n represents the number of observations of the subscripted population) the value of the t statistic can be compared to the t distribution to determine the confidence interval at which the two means can be considered to be different. Here, a confidence interval of 80% or above indicates a statistically significant difference between the mean values of the two populations being compared; a confidence interval of less than 80% suggests that the two population means are not statistically different.

The concentrations of the functional groups change dramatically between the individual trials, and as a result, large 1s errors arise. Because the 1s errors are large, a t test indicates an insignificant difference in the site concentrations of the two species, and an insignificant effect of ionic strength (Table 3). In contrast, the values of the deprotonation constants vary only slightly between trials, and thus they have small corresponding 1s errors. However, because the average values are similar for all titrations modeled, the t test indicates that ionic strength has an insignificant effect, relative to experimental uncertainties, on the magnitudes of the deprotonation constants for both bacterial species. In contrast, the change in the deprotonation constants between the two species at a fixed ionic strength appears significant. In summary, the t test suggests that a single set of parameter values may be adequately applied to all titrations of a given bacteria, regardless of ionic strength, but that the deprotonation constants are species-specific.

Subsequently, we attempt to use a single constant capacitance model to simultaneously fit all four titrations of a given species at a particular ionic strength. The FITEQL results for these net constant capacitance models are listed in Table 4, and in Fig. 3b they are compared to the *B. subtilis* experimental data collected at 0.01 M ionic strength. The model variances are substantially larger when the titrations are modeled simultaneously. This is due to the large variability in the concentrations of surface functional groups observed between the trials. It is apparent from the model variances that *B. licheniformis* is more prone to cell wall variation than *B. subtilis*, as noted by Daughney *et al.* (18). In spite of the apparently poorer fit of these net constant capacitance models, they provide an approximation of the acid–base behavior of each species at each ionic strength. As noted above, the constant capacitance model parameters are, in theory, applicable only to the ionic strength conditions under which they were determined. However, we have shown that the variation in the majority of these parameters is insignificant under the conditions of this study, and thus an average of the parameter values presented in Table 4 may be effectively used to approximate acid–base behavior where species-specific deprotonation constants are not available.

Basic Stern models. We also attempt to model the acid–base behavior of the 16 titrations individually using the basic Stern model. Although Fein *et al.* (17) and Daughney *et al.* (18) have shown that three distinct types of surface sites are required to describe the acid–base behavior of *B. subtilis* and *B. licheniformis*, this conclusion is restricted to the constant capacitance model. Therefore, when using the basic

TABLE 10a

Adsorption of Pb^{2+} by *B. subtilis* as Modeled by FITEQL, Treating Each Bacteria:Metal Ratio Independently

	6.0 g bacteria/L, 10 ppm Pb[b]			3.5 g bacteria/L, 10 ppm Pb			1.5 g bacteria/L, 35 ppm Pb		
Model[a]	Log K_1[c]	Log K_2[d]	$V(Y)$[e]	Log K_1	Log K_2	$V(Y)$	Log K_1	Log K_2	$V(Y)$
				Pb^{2+}–*B. subtilis* adsorption, 0.1 M $NaNO_3$					
C	3.48	—	10.8	4.03	—	58.3	3.93	—	149
P	5.44	—	10.7	5.55	—	0.6	5.75	—	119
H	7.98	—	1.1	8.04	—	2.2	8.37	—	204
C + P	2.69	5.33	1.1	2.76	5.41	0.6		No convergence[f]	
C + H	2.74	7.85	1.1	2.96	2.88	2.3		No convergence	
P + H		No convergence			No convergence		4.58	8.14	37.9
				Pb^{2+}–*B. subtilis* adsorption, 0.01 M $NaNO_3$					
C	3.79	—	3.7	3.66	—	4.6	4.02	—	16.5
P	4.41	—	4.5	4.13	—	0.3	4.11	—	5.1
H	7.58	—	4.7	7.28	—	0.2	6.96	—	5.8
C + P		No convergence			No convergence			No convergence	
C + H		No convergence		2.49	3.43	0.3		No convergence	
P + H		No convergence			No convergence		3.93	4.73	2.8

[a] Models consider adsorption onto one or two distinct types of surface functional groups. C, carboxyl site; P, phosphate site; H, hydroxyl site.
[b] Composition of experimental solutions, indicating mass of bacteria per unit weight of electrolyte and total concentration of metal.
[c] Log K value for metal adsorption onto the first type of surface site included in the model column, referenced to the condition of zero surface charge and zero surface coverage and the ionic strength of the background electrolyte.
[d] Log K value for metal adsorption onto the second type of surface site considered in the model column.
[e] Variance as calculated by FITEQL.
[f] Indicates severe misfit between the model and the experimental data.

Stern model, we attempt to fit the experimental data by considering proton adsorption onto one, two, or three distinct types of surface functional groups, both with and without equilibria describing Na^+ adsorption. As noted above, it is not possible to optimize for the stability constants describing Na^+ adsorption (Eqs. [21]–[23]) and proton adsorption (Eqs. [4]–[6]) simultaneously, in the absence of data describing changes in aqueous Na^+ concentration. Therefore, to test for the effects of Na^+ adsorption, we consider Na^+ adsorption onto the carboxyl, phosphate, and hydroxyl surface sites independently. We fix the values of the deprotonation constants in Eqs. [21]–[23] and optimize for the values of the stability constants in Eqs. [4]–[6]. This procedure is repeated for a range of values for the Na^+ adsorption constants, and the parameter set which best fits the experimental data can be identified.

In Table 5 we provide representative results for the FITEQL basic Stern modeling of two individual *B. subtilis* titrations. Where Na^+ adsorption is not considered, a model invoving two proton-active sites best fits the experimental data. Models considering proton adsorption onto only one type of surface site are characterized by high variances, indicating a poor fit between the model and the experimental data, and models considering proton adsorption onto three types of surface sites fail to converge, indicating that the inclusion of the third site is not warranted by the data. The variances for the two-site basic Stern models are comparable to those of the three-site constant capacitance models given in Table 2, though the basic Stern models predict a much more negative surface potential.

Basic Stern models which consider Na^+ adsorption generally fit the experimental data better than those which do not (Table 5). The experimental data are described equally well by models considering Na^+ adsorption onto any of the three different types of surface sites. However, the log K values describing Na^+ adsorption onto the phosphate and hydroxyl sites are unreasonably large (compared to nonspecific (outer sphere) aqueous Na^+ complexes), and so we consider only Na^+-carboxyl adsorption. In no instance is Na^+ adsorption onto more than one type of surface site required to describe the data. The basic Stern model prediction of surface potential is made less negative if Na^+ adsorption is considered, although the values are still more negative than those predicted by the constant capacticance model. This suggests that low negative surface potential values are required to describe the experimental data. Where Na^+-carboxyl adsorption is considered, the 0.1 M titration data are well described by a model invoking three types of proton-active sites; however, for the 0.01 M titrations, the data are better described by a model involving only two proton-active sites.

TABLE 10b

Adsorption of Pb^{2+} by *B. licheniformis* as Modeled by FITEQL, Treating Each Bacteria:Metal Ratio Independently

	6.0 g bacteria/L, 10 ppm Pb[b]			3.5 g bacteria/L, 10 ppm Pb			1.5 g bacteria/L, 35 ppm Pb		
Model[a]	Log K_1[c]	Log K_2[d]	$V(Y)$[e]	Log K_1	Log K_2	$V(Y)$	Log K_1	Log K_2	$V(Y)$
				Pb^{2+}–*B. licheniformis* adsorption, 0.1 M $NaNO_3$					
C	4.48	—	5.4	4.46	—	5.3	4.54	—	124
P	7.27	—	6.1	7.21	—	2.3	7.43	—	267
H	9.01	—	7.4	8.91	—	2.4	8.07	—	103
C + P		No convergence[f]			No convergence			No convergence	
C + H		No convergence		4.06	8.60	2.3	4.24	7.36	46.5
P + H		No convergence			No convergence		7.34	7.40	38.0
				Pb^{2+}–*B. licheniformis* adsorption, 0.01 M $NaNO_3$					
C	4.11	—	24.9	4.71	—	48.9	4.83	—	48.8
P	6.32	—	20.9	6.25	—	0.7	6.79	—	6.5
H	8.76	—	21.1	8.59	—	1.7	8.58	—	1.1
C + P	4.04	4.57	23.0	2.12	6.24	0.8		No convergence	
C + H	3.87	8.05	22.4	3.69	8.35	1.7	3.30	8.54	1.2
P + H		No convergence		6.24	5.63	0.8	6.37	7.77	0.9

[a] Models consider adsorption onto one or two distinct types of surface functional groups. C, carboxyl site; P, phosphate site; H, hydroxyl site.
[b] Composition of experimental solutions, indicating mass of bacteria per unit weight of electrolyte and total concentration of metal.
[c] Log K value for metal adsorption onto the first type of surface site included in the model column, referenced to the condition of zero surface charge and zero surface coverage and the ionic strength of the background electrolyte.
[d] Log K value for metal adsorption onto the second type of surface site considered in the model column.
[e] Variance as calculated by FITEQL.
[f] Indicates severe misfit between the model and the experimental data.

This difference implies that the basic Stern model invoking Na^+ adsorption cannot account for the observed ionic-strength-dependent changes in proton adsorption. This is further demonstrated in Fig. 5, where a basic Stern model using fit parameters determined from a titration in the 0.1 M electrolyte fails to match the 0.01 M titration data, when adjustments for ionic strength are made. Although Na^+ adsorption may be occurring, and although this may be effectively described by a more complex double-layer model, basic Stern models considering Na^+ adsorption do not effectively describe the data gathered here. Therefore, we select the model with two types of proton-active sites, but without Na^+ adsorption, as the basic Stern model which best describes the experimental data.

Using this two-site basic Stern model, we model each of the 16 individual titrations (Table 6), and we compare the individual model curves to the *B. subtilis* experimental data gathered in the 0.01 M electrolyte (Fig. 3c). The optimizable parameters vary between the individual titrations, for reasons that have been discussed above. Again, we use the Student *t* test for averages to compare the variation in model parameters for the two species in the two different electrolytes (Table 7). The first deprotonation constant appears to be species-specific (at the 95% confidence interval). Variation in the second deprotonation constant between the two species is statistically insignificant. Variation in the surface-site concentrations is also insignificant between the species and between the different ionic strengths. Although some parameters vary significantly between the different titrations, in general, parameter variation between the species and ionic strengths is insignificant, and in this regard, the two-site basic Stern model is in agreement with the constant capacitance model.

We also attempt to use a single two-site basic Stern model to simultaneously fit all four titrations of a given species at a particular ionic strength. The FITEQL results for these net basic Stern models are given in Table 8, and in Fig. 3d they are compared to the *B. subtilis* experimental data collected at 0.01 M ionic strength. Again, the model variances are substantially larger when the titrations are modeled simultaneously, due to the variability in the concentrations of surface functional groups. However, the variation in the model parameters cannot be considered significant, and thus average values (Table 6) can be applied to predict acid-base behavior of the two bacteria in the range of chemical conditions of this study. The net basic Stern model does not describe the experimental data as well as the net constant capacitance model, as indicated by its slightly higher variances. However, because the variances are large in both cases, there is little statistical basis to choose between them.

TABLE 10c

Adsorption of Pb^{2+} by *B. subtilis* and *B. licheniformis* as Modeled by FITEQL, with All Bacteria:Metal Ratios Modeled Simultaneously

	0.1 M $NaNO_3$			0.01 M $NaNO_3$		
Model[a]	Log K_1[b]	Log K_2[c]	$V(Y)$[d]	Log K_1	Log K_2	$V(Y)$
			Pb^{2+}–*B. subtilis* adsorption			
C	3.86	—	82.3	3.85	—	9.3
P	5.60	—	43.0	4.48	—	3.5
H	8.14	—	72.8	7.31	—	4.3
C + P	3.41	5.06	23.2	3.00	4.36	3.6
C + H	3.56	7.22	22.8	3.61	6.07	2.8
P + H	5.50	6.71	10.0	4.45	4.64	3.2
			Pb^{2+}–*B. licheniformis* adsorption			
C	4.53	—	56.7	4.62	—	62.0
P	7.32	—	120	6.42	—	11.5
H	8.45	—	81.6	8.69	—	8.6
C + P	4.40	5.67	33.6	3.41	6.32	11.3
C + H	4.36	4.74	22.9	3.67	8.42	8.3
P + H	No convergence[e]			6.25	7.78	8.4

[a] Models consider adsorption onto one or two distinct types of surface functional groups. C, carboxyl site; P, phosphate site; H, hydroxyl site.

[b] Log K value for metal adsorption onto the first type of surface site included in the model column, referenced to the condition of zero surface charge and zero surface coverage and the ionic strength of the background electrolyte.

[c] Log K value for metal adsorption onto the second type of surface site considered in the model column.

[d] Variance as calculated by FITEQL.

[e] Indicates severe misfit between the model and the experimental data.

Finally, we attempt to use the two-site basic Stern model to simultaneously describe all eight titrations for each species, including trials performed at different solid:solution ratios and both ionic strengths. Such a model fails to converge for the *B. subtilis* titration data, although it provides a slightly improved fit for the *B. licheniformis* data. Because the applicability of this model is not adequate for both species, we favor the net constant capacitance model.

Consideration of errors. The relative 1*s* errors associated with the log deprotonation constants and site concentrations reported here are approximately ±6 and ±60%, respectively. These errors arise from three principal sources. First, we consider the analytical error associated with our method of titration. We have examined the accuracy of this experimental technique by reproducing the deprotonation constant and total concentration of functional groups in a sodium acetate system, to within 2% of the expected values (the literature pK_a value and initial acetate concentration, respectively). We conclude that the deprotonation constants and concentrations of the bacterial functional groups reported here carry maximum relative 1*s* errors of ±2% due to analytical uncertainties.

Second, the variables required for the electric double-layer models (surface area and mass of bacteria per unit weight of electrolyte) are difficult to quantify, and so give rise to errors in the model parameters. The BET and organic adsorption techniques commonly used to determine surface area cannot be applied to bacteria because both techniques markedly alter the cell wall. We determine the bacterial surface area from cell geometry. The cell surface area of these rod-shaped species is approximately equal to that of a right circular cylinder with spherical ends, of length 5.0 μm and radius 0.5 μm. There are approximately 4×10^9 cells per gram of bacteria (17). These values yield a bacterial surface area of approximately 140 m^2/g, although errors in the cell dimensions, surface roughness, and quantity of cells per gram cause this estimate to vary over roughly one order of magnitude. Changes in the model surface area values between 50 and 500 m^2/g cause the surface-site concentrations to vary by approximately ±5% and the deprotonation constants to change by roughly ±1%. Additionally, the bacteria may multiply during the experiments, giving rise to an error in the mass or surface area of bacteria per unit mass of suspension that we apply in our modeling. We have examined this possibility by separating and drying the bacteria in the suspension both prior to and following the titrations. We observe no increase in the weight of bacteria present, and thus we consider this error to be negligible. Finally, the bacterial biomass per unit weight of electrolyte is determined by separating the bacteria from a known weight of electrolyte through centrifugation (6000 rpm for 60 min) and weighing the pellet produced. The centrifugation may not effectively remove all the electrolyte solution or, alternatively, fluids may be driven out of the cells, and so the weight of bacteria determined carries a 1*s* error of roughly ±5%. This error in bacterial biomass, when propagated through the FITEQL models, causes errors in the log deprotonation constants and site concentrations of ±2 and ±5%, respectively. Thus the surface-site concentrations determined here carry 1*s* errors of ±10% due to inaccuracies in the values of bacterial mass and surface area applied in the modeling, while the log deprotonation constants carry errors of ±4%.

Third, the accuracy of the models developed here depends on the extent of cell wall variation between cultures. As described above, the cell wall characteristics of independently grown cultures of *B. subtilis* and *B. licheniformis* appear to vary substantially. Cell wall variation seems to cause little variation in the log deprotonation constants (±2%), but is likely responsible for the majority of the error (±45–50%) in the surface-site concentrations. Variations in the surface-site concentrations are large and essentially random, and they are the greatest limitation to the develop-

TABLE 11a

Adsorption of Cu^{2+} by *B. subtilis* as Modeled by FITEQL, Treating Each Bacteria:Metal Ratio Independently

	6.0 g bacteria/L, 10 ppm Cu[b]			3.5 g bacteria/L, 10 ppm Cu			1.5 g bacteria/L, 15 ppm Cu		
Model[a]	Log K_1[c]	Log K_2[d]	$V(Y)$[e]	Log K_1	Log K_2	$V(Y)$	Log K_1	Log K_2	$V(Y)$
				Cu^{2+}–*B. subtilis* adsorption, 0.1 M $NaNO_3$					
C	3.73	—	21.2	3.80	—	75.1	4.00	—	115
P	5.82	—	24.6	5.71	—	10.8	5.68	—	86.2
H	8.38	—	22.9	8.33	—	18.9	8.36	—	178
C + P	3.67	4.53	19.4		No convergence[f]			No convergence	
C + H	3.68	6.88	20.1		No convergence			No convergence	
P + H		No convergence		5.54	7.40	9.5	5.34	6.51	26.2
				Cu^{2+}–*B. subtilis* adsorption, 0.01 M $NaNO_3$					
C	3.67	—	21.8	3.95	—	44.3	4.22	—	323
P	4.61	—	11.3	4.51	—	12.7	4.22	—	108
H	7.49	—	14.5	7.31	—	21.5	7.05	—	129
C + P	3.37	4.21	8.3	3.47	4.15	7.6		No convergence	
C + H	3.42	7.02	8.3	3.57	6.88	8.4	3.62	6.48	115
P + H		No convergence			No convergence		4.07	5.98	101

[a] Models consider adsorption onto one or two distinct types of surface functional groups. C, carboxyl site; P, phosphate site; H, hydroxyl site.
[b] Composition of experimental solutions, indicating mass of bacteria per unit weight of electrolyte and total concentration of metal.
[c] Log K value for metal adsorption onto the first type of surface site included in the model column, referenced to the condition of zero surface charge and zero surface coverage and the ionic strength of the background electrolyte.
[d] Log K value for metal adsorption onto the second type of surface site considered in the model column.
[e] Variance as calculated by FITEQL.
[f] Indicates severe misfit between the model and the experimental data.

ment of a single predictive model to describe the acid–base behavior of these bacterial surfaces.

Summary and choice of model. A comparison of the variances listed in Tables 2 and 6 indicates that the three-site constant capacitance model provides a better description of acid–base behavior than the two-site basic Stern model, when the titrations are modeled independently. Further, the addition of the third surface site in the constant capacitance model is justified by experimental studies which indicate that the cell walls of these bacteria display carboxyl, phosphate, and hydroxyl functional groups (13). Thus we favour the constant capacitance model over the basic Stern model where the titrations are modeled individually.

The experimental data are better described when the titrations are modeled individually than when several titrations are modeled simultaneously, but because the optimizable parameters of individual titrations vary substantially, an average set of parameter values is better used to predict the acid–base behavior of the bacterial suspensions. A comparison of the variances listed in Tables 2, 4, 6, and 8 shows that simultaneous modeling of several titrations yields a set of parameters that closely agrees with the averages of the parameters determined when the titrations are modeled individually. Further, the net constant capacitance models describe the experimental data slightly better than the net basic Stern models. It has also been shown above that the deprotonation constants are species-specific. Therefore, we choose to model acid–base behavior using the four parameter sets given in Table 4, one set corresponding to each bacteria in each electrolyte, rather than applying average parameter values.

METAL ADSORPTION RESULTS AND DISCUSSION

The results of the Cd^{2+}, Pb^{2+}, and Cu^{2+} adsorption experiments are displayed in Figs. 6 to 8, respectively. All of the adsorption experiments were performed below saturation with respect to any solid metal phase, and so any change in the aqueous metal concentration observed during the experiment is attributed entirely to adsorption onto the cell wall. It is evident that the bacterial cell walls display a strong affinity for the metals used in this study, with the extent of metal adsorption increasing with increasing pH. Further, the proportion of metal adsorbed at a particular pH increases as the ratio between the total concentration of bacterial surface functional groups and the total metal concentration (bacteria:metal ratio) increases. These results are in excellent agreement with those of Fein *et al.* (17) and Daughney *et al.* (18). Generally, the positions of the metal–*B. subtilis* adsorption edges are shifted to lower pH values when the

TABLE 11b

Adsorption of Cu^{2+} by *B. licheniformis* as Modeled by FITEQL, Treating Each Bacteria:Metal Ratio Independently

	6.0 g bacteria/L, 10 ppm Cu[b]			3.5 g bacteria/L, 10 ppm Cu			1.5 g bacteria/L, 15 ppm Cu		
Model[a]	Log K_1[c]	Log K_2[d]	$V(Y)$[e]	Log K_1	Log K_2	$V(Y)$	Log K_1	Log K_2	$V(Y)$
				Cu^{2+}–*B. licheniformis* adsorption, 0.1 M $NaNO_3$					
C	4.68	—	18.4	4.93	—	33.6	4.54	—	133
P	7.71	—	19.8	8.02	—	307	7.43	—	411
H	9.18	—	36.8	9.37	—	18.9	8.19	—	76.3
C + P		No convergence[f]			No convergence			No convergence	
C + H		No convergence		4.79	8.42	13.5	4.18	7.37	18.5
P + H	7.71	5.58	21.0	7.67	8.74	15.8		No convergence	
				Cu^{2+}–*B. licheniformis* adsorption, 0.01 M $NaNO_3$					
C	4.15	—	23.8	4.90	—	390	3.05	—	14.1
P	6.46	—	139	6.84	—	91.2	4.20	—	6.8
H	8.87	—	150	7.36	—	47.3	6.36	—	3.4
C + P	4.12	3.72	24.1	3.06	6.81	97.8		No convergence	
C + H	4.13	5.82	24.4	4.11	7.02	14.1		No convergence	
P + H		No convergence		6.50	6.49	18.7		No convergence	

[a] Models consider adsorption onto one or two distinct types of surface functional groups. C, carboxyl site; P, phosphate site; H, hydroxyl site.
[b] Composition of experimental solutions, indicating mass of bacteria per unit weight of electrolyte and total concentration of metal.
[c] Log K value for metal adsorption onto the first type of surface site included in the model column, referenced to the condition of zero surface charge and zero surface coverage and the ionic strength of the background electrolyte.
[d] Log K value for metal adsorption onto the second type of surface site considered in the model column.
[e] Variance as calculated by FITEQL.
[f] Indicates severe misfit between the model and the experimental data.

ionic strength is decreased. In contrast, the metal–*B. licheniformis* adsorption edges are shifted to higher pH values when the ionic strength is decreased.

For each metal–bacteria system, we use FITEQL to solve for site-specific stability constants describing metal adsorption onto the bacterial cell walls (Tables 9–11). We attempt to fit the experimental data by invoking models involving metal adsorption onto one, two, or three distinct types of surface functional groups. Models considering adsorption onto three distinct surface sites generally fail to converge, suggesting that the inclusion of the third equilibrium does not improve the goodness of fit, and therefore such models are not tabulated here. We consider only the 1:1 stoichiometry for the adsorbed metal surface complex, after Fein *et al.* (17) and Daughney *et al.* (18). Equilibria describing metal hydrolysis are included in our models, with stability constants taken from Baes and Mesmer (40). In our FITEQL modeling, we use the net constant capacitance model parameters given in Table 4, applying a separate parameter set for each bacterial species at each ionic strength. For each metal, we first model the experimental data for the suspensions of 1.5, 3.5, and 6.0 g bacteria/L independently. Subsequently, we model the experimental data for all three bacteria:solution ratios simultaneously, in order to determine a single set of stability constants describing metal adsorption in systems of different bacteria:solution ratios. The metal adsorption stability constants reported here are referenced to zero surface charge, zero surface coverage, and the ionic strength of the background electrolyte.

One-site metal adsorption models. We first describe the experimental data by considering metal adsorption onto only one type of surface functional group. It is important to note that the fit of any given model depends on three mathematical and logistical constraints, over and above its relationship to the chemical processes that it attempts to describe. As a result, the fit of any one-site model is variable, as indicated by the range of variances listed in Tables 9–11. First, the fit of these models is largely controlled by the concentration of bacteria present. Where the concentration of bacteria is highest, the adsorption edge is steep, and a one-site model can provide a good fit to the experimental data. In contrast, where the bacterial concentration is low, the metal can saturate one type of surface site, with excess metal available to adsorb onto the next surface site which deprotonates. Under these conditions, adsorption occurs over a pH range in which two types of surface functional groups actively deprotonate, and the metal adsorption edge is less steep. In such cases, the one-site models fit the data poorly. Because of this, where the data for all bacteria concentrations are considered simultaneously, the one-site models often indicate a relatively

TABLE 11c

Adsorption of Cu^{2+} by *B. subtilis* and *B. licheniformis* as Modeled by FITEQL, with All Bacteria:Metal Ratios Modeled Simultaneously

	0.1 M $NaNO_3$			0.01 M $NaNO_3$		
Model[a]	Log K_1[b]	Log K_2[c]	$V(Y)$[d]	Log K_1	Log K_2	$V(Y)$
			Cu^{2+}–*B. subtilis* adsorption			
C	3.83	—	76.0	3.84	—	145
P	5.75	—	39.5	4.56	—	42.2
H	8.35	—	69.5	7.35	—	61.2
C + P	3.55	4.94	28.8	3.20	4.36	42.0
C + H	3.59	7.34	28.1	5.01	6.68	41.6
P + H	4.25	8.30	23.5	4.53	5.79	40.0
			Cu^{2+}–*B. licheniformis* adsorption			
C	4.82	—	69.2	4.30	—	224
P	7.06	—	240	6.40	—	146
H	9.05	—	128	8.69	—	164
C + P	4.73	5.70	47.8	3.93	5.51	138
C + H	4.75	7.19	45.0	6.31	6.89	51.9
P + H	No convergence[e]			9.70	6.47	120

[a] Models consider adsorption onto one or two distinct types of surface functional groups. C, carboxyl site; P, phosphate site; H, hydroxyl site.

[b] Log K value for metal adsorption onto the first type of surface site included in the model column, referenced to the condition of zero surface charge and zero surface coverage and the ionic strength of the background electrolyte.

[c] Log K value for metal adsorption onto the second type of surface site considered in the model column.

[d] Variance as calculated by FITEQL.

[e] Indicates severe misfit between the model and the experimental data.

poor fit to the data (the variance and best-fit stability constant for these models are essentially averages of the values determined when the different bacteria concentrations are modeled independently). Therefore, the appropriateness of any one-site model is best evaluated by considering its fit to the data for the highest bacteria concentration, before considering its fit to the data for all bacteria concentrations modeled simultaneously.

Second, the fit of any one-site model is controlled by the position of the metal adsorption edge as a function of pH. For example, the 0.1 M Cd^{2+}–*B. subtilis* adsorption edge occurs over a pH range where the phosphate surface sites are significantly deprotonated, and thus a model considering Cd^{2+} adsorption onto the phosphate sites fits the data well. By contrast, the 0.01 M Cd^{2+}–*B.subtilis* adsorption edge occurs at a slightly lower pH, and so the experimental data are better described by adsorption onto the carboxyl surface sites. For similar reasons, Cd^{2+} adsorption onto *B. licheniformis* in the 0.1 M electrolyte can be modeled by adsorption onto the phosphate sites, but because a decrease in ionic strength causes the adsorption edge to shift up with respect to pH, the 0.01 M Cd^{2+}–*B. licheniformis* data are better described by adsorption onto the hydroxyl sites.

Third, it is also important to note that the two species of bacteria have different deprotonation constants for each type of surface functional group. The phosphate sites on *B. subtilis* begin to deprotonate at a lower pH than those on *B. licheniformis,* and as a result, metal–phosphate adsorption models will only fit the *B. licheniformis* data if the metal adsorption edge occurs over a pH of approximately 5.5–6.5. With the above discussion in mind, it is possible to compare the appropriateness of the various one-site models.

The one-site models invoking metal adsorption onto either the carboxyl or the phosphate surface sites fit the experimental data equally well. However, research indicates that Cu^{2+} and other hard metal cations (Na^+, Mg^{2+}, Mn^{2+}, Fe^{3+}) are preferentially bound to carboxyl sites on the cell walls of both *B. subtilis* and *B. licheniformis* (13, 41, 42). Further, it is known that metal ions display a similar affinity series for a given group of ligands regardless of whether the ligands exist as surface functional groups or as aqueous species (25). For the systems examined here, the magnitudes of the metal adsorption constants indicate that Cd^{2+} has the lowest affinity for the bacterial surface, while Pb^{2+} and Cu^{2+} have greater but roughly equal affinities for the bacterial surface. This same affinity series also describes the complexation of Cd^{2+}, Pb^{2+}, and Cu^{2+} by aqueous carboxylate anions (36). This agreement between the affinity series for metal–bacteria adsorption and metal–carboxylate complexation suggests that metal–bacteria adsorption involves carboxyl surface functional groups. An examination of the adsorption data (Figs. 6 to 8) indicates that adsorption is generally initiated well below the pH at which the phosphate sites are significantly deprotonated. Therefore, it is most likely that metal–carboxyl interactions are responsible for the observed adsorption behavior. Note that the association of an adsorbed metal ion with a particular type of functional group has not been directly observed in this study, but rather inferred from the experimental data. Confirmation of the model selected here requires direct observation of the adsorbed metals.

Two-site metal adsorption models. Although some of the experimental data can be described by models considering adsorption onto only the carboxyl surface sites, for the majority of metal–bacteria systems examined here, a better fit to the data is obtained by a model which considers metal adsorption onto two types of surface functional groups (Tables 9–11). Note that the improved fit may be the result of the addition of an additional optimizable parameter to the model. Two types of two-site models provide close fits to the experimental data, the first considering adsorption onto the carboxyl and phosphate sites, and the second considering adsorption onto the carboxyl and hydroxyl sites. The former type of model is more chemically meaningful,

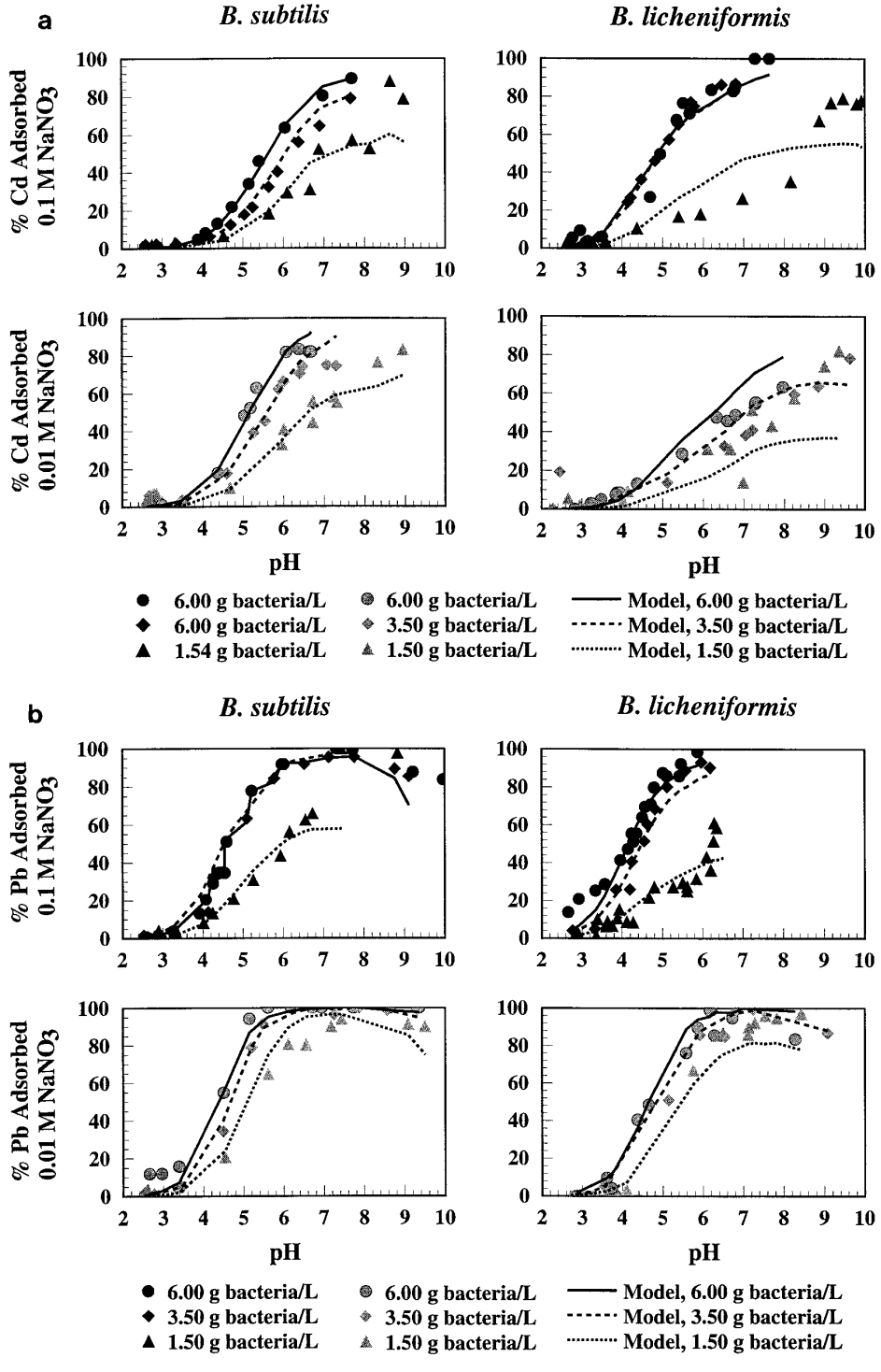

FIG. 9. FITEQL model curves describing adsorption of (a) Cd^{2+}, (b) Pb^{2+}, and (c) Cu^{2+} onto *B. subtilis* and *B. licheniformis* in 0.1 M $NaNO_3$ (black symbols) and 0.01 M $NaNO_3$ (gray symbols). Model curves consider metal adsorption onto carboxyl and phosphate sites.

because the phosphate sites are significantly deprotonated in the pH range where the adsorption edge occurs, while the hydroxyl sites are not. We therefore select the model considering adsorption onto the carboxyl and phosphate sites as the two-site model which best describes the experimental data, in agreement with Fein *et al.* (17) and Daughney *et al.* (18). These models are compared to the experimental data in Fig. 9.

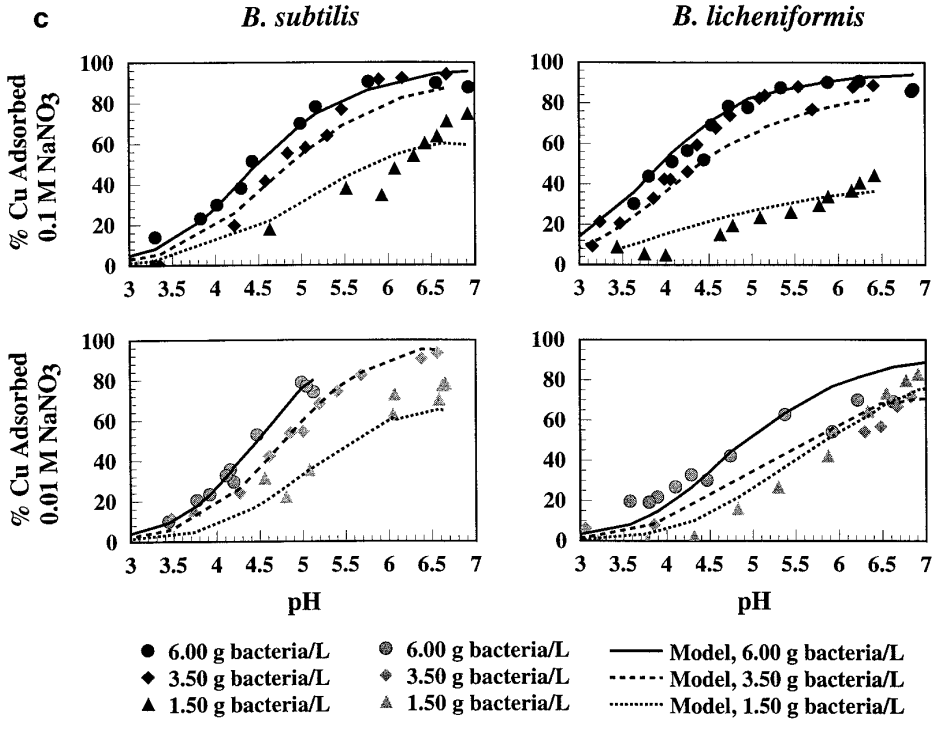

FIG. 9—*Continued*

Three trends are recognizable in the magnitudes of the stability constants presented in Tables 9–11. First, for both bacterial species, at both ionic strengths, Cd^{2+} has the lowest affinity for the surface, followed by Pb^{2+}, followed by Cu^{2+}, which has the highest affinity for the surface. The stability constants reported here are in good general agreement with those reported by Fein *et al.* (17) and Daughney *et al.* (18) (Table 1). The discrepancy in the values of the stability constants given in Tables 1 and 9–11 is likely due to differences in the parameters used to characterize the acid–base behavior of the bacterial surfaces. The metal adsorption stability constants given here should therefore be applied in combination with the surface parameters provided in Table 4.

Second, for a given ionic strength, the metal–carboxyl and metal–phosphate stability constants for *B. licheniformis* are greater than those for *B. subtilis.* As noted by Daughney *et al.* (18), there is an excellent correlation between the magnitudes of the metal–carboxyl stability constants describing adsorption onto *B. subtilis* and *B. licheniformis* (Fig. 10). The correlation between the metal–phosphate stability constants is also very good. This correlation suggests that metal–carboxyl stability constants for one species of bacteria can be estimated if the stability constant describing adsorption of the same metal onto a different type of bacteria has been measured. The slopes of the majority of the correlation lines are similar, suggesting that the correlation parameters presented in Fig. 10 may be applied to ionic strengths different from those used here.

Third, for both bacterial species, the metal–carboxyl and metal–phosphate stability constants generally decrease with

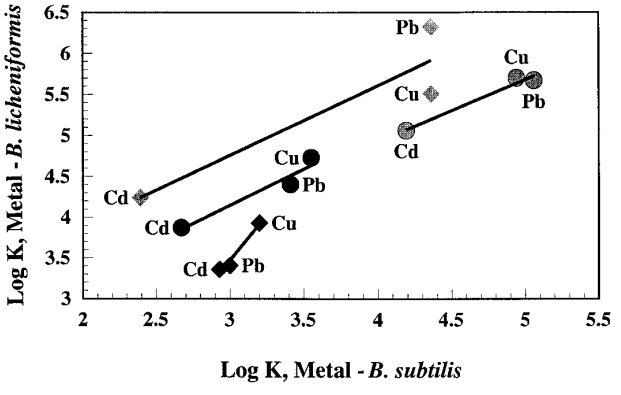

Metal-Carboxyl Correlation, 0.1 M	y = 1.474 + 0.891x	R^2 = 0.97
Metal-Carboxyl Correlation, 0.01 M	y = -3.187 + 2.219x	R^2 = 0.99
Metal-Phosphate Correlation, 0.1 M	y = 1.905 + 0.755x	R^2 = 0.99
Metal-Phosphate Correlation, 0.01 M	y = 2.208 + 0.850x	R^2 = 0.92

FIG. 10. Correlation diagram relating metal–carboxyl and metal–phosphate stability constants of *B. subtilis* and *B. licheniformis,* at 0.1 and 0.01 M $NaNO_3$. The equation of the linear regression line and the linear correlation coefficient are shown.

decreasing ionic strength. This ionic strength dependence suggests that metal adsorption is affected by the bacterial surface charge, which, if compared to studies of ion adsorption by mineral surfaces (27, 43), may indicate that the adsorbed metals exist as outer-sphere surface complexes. However, the decrease in the values of the metal–bacteria stability constants with decreasing ionic strength is a trend opposite to that observed for metal adsorption onto most mineral surfaces (27, 43), which implies that the surface complexes may have a different form or structure than that assumed here. Further, the two species of bacteria behave differently in terms of the extent of metal they adsorb as ionic strength is changed. The *B. licheniformis* experimental data indicate that, at a given pH, adsorption decreases with decreasing ionic strength. The *B. subtilis* adsorption data, however, show an opposite trend, which is not reflected as a change in stability constants as a function of ionic strength. The magnitude of the change in the stability constants is too large and too variable to be caused by changes in the activity of the metal ion in the different electrolyte solutions. It is possible that the two species adsorb Na^+ differently as ionic strength changes, leading to differences in surface potential which give rise to the trends observed here. However, the data collected in this study do not permit the determination of stability constants describing electrolyte adsorption. Nonetheless, this suggests that the near-surface region may have different characteristics than assumed here. Spectroscopic studies are required to clarify the structure of the adsorbed metals and electrolyte ions. Pending the collection of such data, metal adsorption onto the carboxyl and phosphate surface sites is best modeled with the stability constant values summarized in Table 12.

TABLE 12
Summary of Stability Constants Describing Adsorption of Cd, Pb, and Cu onto *B. subtilis* and *B. licheniformis*

	0.1 M $NaNO_3$		0.01 M $NaNO_3$	
Metal[a]	Log *K* M-carboxyl[a]	Log *K* M-phosphate[b]	Log *K* M-carboxyl	Log *K* M-phosphate
		B. subtilis		
Cd	2.67	4.19	2.93	2.39
Pb	3.41	5.06	3.00	4.36
Cu	3.55	4.94	3.20	4.36
		B. licheniformis		
Cd	3.87	5.06	3.36	4.24
Pb	4.40	5.67	3.41	6.32
Cu	4.73	5.70	3.93	5.51

[a] Log *K* value for metal adsorption onto the carboxyl surface sites, referenced to the condition of zero surface charge and zero surface coverage and the ionic strength of the background electrolyte.

[b] Log *K* value for metal adsorption onto the phosphate surface sites. Stability constants are determined by modeling all bacteria:metal ratios simultaneously.

CONCLUSIONS

This results of this study illustrate that the surface characteristics of *B. subtilis* and *B. licheniformis* are affected by changes in solution ionic strength. The surface properties and acid–base behavior of the two bacterial species can be modeled in the framework of chemical thermodynamics, with a different set of stability constants describing interactions between protons and the distinct functional groups on the cell walls. The changes in surface characteristics and metal-binding capacities associated with changes in solution ionic strength are manifested by changes in the magnitudes of the site concentrations and deprotonation constants included in the chemical models. We find that the constant capacitance model is more effective than the basic Stern model in its ability to describe ionic-strength-dependent acid–base behavior.

The adsorption of Cd^{2+}, Pb^{2+}, and Cu^{2+} onto *B. subtilis* and *B. licheniformis* is also controlled by ionic strength, as indicated by variation in the stability constants describing metal adsorption in different electrolytes. Metal adsorption is best described by models considering adsorption onto both the carboxyl and the phosphate functional groups. The changes in the metal adsorption stability constants show systematic variation with ionic strength, bacterial species, and metal involved. Therefore, the model parameters provided here may be applied to predict metal adsorption in solutions which are different from those of this study, providing the bacteria are cultured and prepared as described above. Spectroscopic studies of the bacterial surfaces are recommended in order to elucidate more precisely the nature of the adsorbed metal complexes. Additional research is required to model proton and metal adsorption in natural environments, where many species of bacteria may be present, where cell wall characteristics may change with growth conditions, and where cell wall fragments and extracellular dissolved organics may compete for available cations.

ACKNOWLEDGMENTS

This work was funded by an NSERC Operating Grant and a FCAR Nouveaux Chercheurs Grant to J.B.F. We thank Alfonso Mucci for the use of his autotitrator and Nathan Yee for performing some of the metal adsorption experiments. This communication was improved with the careful editing of an anonymous reviewer.

REFERENCES

1. Geesey, G. G., Richardson, W. T., Yeomans, H. G., Irvin, R. T., and Costerton, J. W., *Can. J. Microbiol.* **23,** 1733 (1977).

2. Harvey, R. W., and Young, L. Y., *Appl. Environ. Microbiol.* **39,** 894 (1980).
3. Lion, L. W., and Leckie, J. O., *Annu. Rev. Earth Planet. Sci.* **9,** 449 (1981).
4. Jannasch, H. W., and Mottl, M. J., *Science* **229,** 717 (1985).
5. Yayanos, A. A., *Proc. Natl. Acad. Sci. USA* **83,** 9542 (1986).
6. Ghiorse, W. S., and Wilson, J. T., *Adv. Appl. Microbiol.* **33,** 197 (1988).
7. Huber, R., Stoffers, P., Cheminee, J. L., Richnow, H. H., and Stetter, K. O., *Nature* **345,** 179 (1990).
8. Mahmood, S. K., and Rama, R. P., *Environ. Contam. Toxicol.* **50,** 486 (1993).
9. Yakimov, M. M., Timmis, K. N., Wray, V., and Fredrickson, H. L., *Appl. Environ. Microbiol.* **61,** 1706 (1995).
10. Davis, J. A., *Geochim. Cosmochim. Acta* **48,** 679 (1984).
11. Schlautman, M. A., and Morgan, J. J., *Geochim. Cosmochim. Acta* **58,** 4293 (1994).
12. Beveridge, T. J., and Murray, R. G. E., *J. Bacteriol.* **127,** 1502 (1976).
13. Beveridge, T. J., and Murray, R. G. E., *J. Bacteriol.* **141,** 876 (1980).
14. Beveridge, T. J., and Koval, S. F., *Appl. Environ. Microbiol.* **42,** 325 (1981).
15. Gonçalves, M. L. S., Sigg, L., Reutlinger, M., and Stumm, W., *Sci. Total Environ.* **60,** 105 (1987).
16. Beveridge, T. J., *Annu. Rev. Microbiol.* **43,** 147 (1989).
17. Fein, J. B., Daughney, C. J., Yee, N., and Davis, T., [submitted for publication]
18. Daughney, C. J., Fein, J. B., and Yee, N., [submitted for publication]
19. Corapcioglu, M. Y., and Kim, S., *Water Res.* **31,** 2693 (1995).
20. Ferris, F. G., Fyfe, W. S., and Beveridge, T. J., *Geology* **16,** 149 (1988).
21. Savvichev, A. S., Nikitin, D. I., and Oranskaya, M. S., *Geochem. Int.* **23,** 60 (1986).
22. Plette, A. C. C., Van Reimsdijk, W. H., Bendetti, M. F., and Van der Wal, A., *J. Coll. Interface Sci.* **173,** 354 (1995).
23. Harden, V. P., and Harris, J. O., *J. Bacteriol.* **65,** 198 (1953).
24. Stumm, W., and Morgan, J. J., ''Aquatic Chemistry,'' 3rd ed. Wiley, NY, 1996.
25. Langmuir, D., ''Aqueous Environmental Geochemistry.'' Prentice-Hall, NJ, 1997.
26. Westall, J., and Hohl, H., *Adv. Colloid Interface Sci.* **12,** 265 (1980).
27. Davis, J. A., and Kent, D. B., *in* ''Mineral-Water Interface Geochemistry'' (M. F. Hochella and A. F. White, Eds.), Reviews in Mineralogy, Vol. 23, p. 177. Mineralogical Society of America, 1990.
28. Duncan, K. E., Ferguson, N., Kimura, K., Zhou, X., and Istock, C. A., *Evolution* **48,** 2002 (1994).
29. Collins, Y. E., and Stotzky, G., *Appl. Environ. Microbiol.* **58,** 1592 (1991).
30. Hohl, H., and Stumm, W., *J. Colloid Interface Sci.* **55,** 281 (1976).
31. Stern, O., *Z. Elektrochem.* **30,** 508 (1924).
32. Hayes, K. F., Redden, G., Wendell, E., and Leckie, J. O., *J. Colloid Interface Sci.* **142,** 448 (1991).
33. Katz, L. E., and Hayes, K. F., *J. Colloid Interface Sci.* **170,** 477 (1995).
34. Westall, J., ''FITEQL. A Computer Program for Determination of Chemical Equilibrium Constants from Experimental Data.'' Department of Chemistry, Oregon State Univ., Report 82-01, 1982a.
35. Westall, J., ''FITEQL. A Computer Program for Determination of Chemical Equilibrium Constants from Experimental Data.'' Department of Chemistry, Oregon State Univ., Report 82-02, 1982b.
36. Smith, R. M., and Martell, A. E., ''Critical Stability Constants. IV: Inorganic Complexes.'' Plenum, NY, 1976.
37. Herben, P. F. G., Mozes, N., and Rouxhet, P. G., *Biochem. Biophys. Acta* **1033,** 184 (1990).
38. Brock, T. D., and Madigan, M. T., ''Biology of Microorganisms.'' Prentice Hall, NJ, 1970.
39. Neter, J., Wasserman, W., and Whitmore, G. A., ''Applied Statistics.'' Allyn & Bacon, MA, 1988.
40. Baes, C. F., and Mesmer, R. E., ''The Hydrolysis of Cations.'' Wiley-Interscience, NY, 1976.
41. Doyle, R. J., Matthews, T. H., and Strepis, U. N., *J. Bacteriol.* **143,** 471 (1980).
42. Beveridge, T. J., Forsberg, C. W., and Doyle, R. J., *J. Bacteriol.* **150,** 1438 (1982).
43. Parks, G. A. *in* ''Mineral-Water Interface Geochemistry'' (M. F. Hochella and A. F. White, Eds.), Reviews in Mineralogy, Vol. 23, p. 133. Mineralogical Society of America, 1990.